2014

Plant defense suppression is mediated by a fungal sirtuin during rice infection by *Magnaporthe oryzae*

Jessie Fernandez
University of Nebraska-Lincoln, jfernandez99@huskers.unl.edu

Margarita Marroquin-Guzman
University of Nebraska-Lincoln, mmarroquinguzman2@unl.edu

Renu Nandakumar
University of Nebraska-Lincoln, rnandakumar2@unl.edu

Sara Shijo
University of Nebraska-Lincoln

Kathryn M. Cornwell
University of Nebraska-Lincoln

See next page for additional authors

Published in *Molecular Microbiology* 94:1 (2014), pp 70–88.
doi:10.1111/mmi.12743
PMID: 25098820

Accepted 31 July, 2014. Published 21 August 2014.

Plant defense suppression is mediated by a fungal sirtuin during rice infection by *Magnaporthe oryzae*

Jessie Fernandez,[1] Margarita Marroquin-Guzman,[1] Renu Nandakumar,[2] Sara Shijo,[1] Kathryn M. Cornwell,[1] Gang Li,[1] and Richard A. Wilson[1]

1 Department of Plant Pathology, University of Nebraska-Lincoln, Lincoln, NE 68583, USA
2 Proteomic and Metabolomic Core Facility, Redox Biology Center, Department of Biochemistry, University of Nebraska-Lincoln, Lincoln, NE 68588, USA

Corresponding author — R. A. Wilson, *email* rwilson10@unl.edu

Present address for J. Fernandez — University of Texas Southwestern Medical Center, 5323 Harry Hines Blvd, Dallas, TX 75390, USA

Abstract

Crop destruction by the hemibiotrophic rice pathogen *Magnaporthe oryzae* requires plant defense suppression to facilitate extensive biotrophic growth in host cells before the onset of necrosis. How this is achieved at the genetic level is not well understood. Here, we report that a *M. oryzae* sirtuin, MoSir2, plays an essential role in rice defense suppression and colonization by controlling superoxide dismutase (SOD) gene expression. Loss of MoSir2 function in Δ*sir2* strains did not affect appressorial function, but biotrophic growth in rice cells was attenuated. Compared to wild type, Δ*sir2* strains failed to neutralize plant-derived reactive oxygen species (ROS) and elicited robust defense responses in rice epidermal cells that included elevated pathogenesis-related gene expression and granular depositions. Deletion of a SOD-encoding gene under MoSir2 control generated Δ*sod1* deletion strains that mimicked Δ*sir2* for impaired rice defense suppression, confirming SOD activity as a downstream output of MoSir2. In addition, comparative protein acetylation studies and forward genetic analyses identified a JmjC domain-containing protein as a likely target of MoSir2, and a Δ*sir2* Δ*jmjc* double mutant was restored for *MoSOD1* expression and defense suppression in rice epidermal cells. Together, this work reveals MoSir2 and MoJmjC as novel regulators of early rice cell infection.

Introduction

Fungal pathogens of plants seek to access host nutrients in order to propagate their disease cycle and thus represent significant threats to global food security (Fisher *et al*., 2012). To achieve this goal, fungi have adopted several lifestyles in order to invade, overcome and exploit their hosts. Biotrophs (reviewed in Spanu, 2012), such as those fungi causing rusts and powdery mildews, need living tissue to survive, while necrotrophs (reviewed in Laluk and Mengiste, 2010) such as *Botrytis cinerea* kill the host to acquire nutrients. Hemibiotrophs (Perfect and Green, 2001; Koeck *et al*., 2011), including the rice blast fungus *Magnaporthe oryzae*, grow asymptomatically within living plant cells as a biotroph before switching to a necrotrophic stage. Recent progress has been made in understanding the biological processes employed by *M. oryzae* during biotrophy – such as the secretion of effectors to condition the host cell for invasion (Wilson and Talbot, 2009; Koeck *et al*., 2011; Fernandez and Wilson, 2012; Giraldo *et al*., 2013; Yi and Valent, 2013) – but the underlying regulatory factors are largely unknown (Fernandez *et al*., 2012; 2013; Fernandez and Wilson, 2014a).

Magnaporthe oryzae is the most serious disease of cultivated rice (Wilson and Talbot, 2009). It accesses host cells using a pressurized dome-shaped cell, the appressorium (Dagdas *et al*., 2012), which develops on the surface of the leaf, breaches the rice cuticle, and proceeds to elaborate bulbous invasive hyphae (IH) that first colonize the underlying epidermal cells (Fernandez and Wilson, 2014a). For the first 4–6 days of infection, *M. oryzae* spreads from cell-to-cell as a symptomless biotroph (Kankanala *et al*., 2007) before necrotic lesions appear on the leaf surface. During early infection, growth in host cells is facilitated by the secretion of apoplastic and cytoplasmic effectors with likely roles in suppressing host defenses and/or altering the host cell environment to the benefit of the fungus (Mosquera *et al*., 2009; Khang *et al*., 2010; Giraldo *et al*., 2013). In addition, the host produces a burst of reactive oxygen species (ROS) in response to *M. oryzae* infection, and this has to be neutralized in order for rice cell infection to occur. The inability of the *M. oryzae* mutants Δ*des1* (Chi *et al*., 2009) and Δ*hyr1* (Huang *et al*., 2011) to neutralize host-derived ROS resulted in elevated plant defense responses that included increased pathogenesis-related (PR) gene expression and granular depositions in the host cell.

Recently, two related regulatory processes, critical to nutrient adaptation and host infection, have recently been described in *M. oryzae*: an NADPH-dependent switch (Wilson *et al*., 2010), which uses NADPH produced in response to glucose-6-phosphate (G6P) sensing by trehalose-6-phosphate synthase 1 (Tps1; Wilson *et al*., 2007) to control the activity of several GATA transcription factors, including the nitrogen regulator Nut1 (Fernandez and Wilson, 2012); and carbon catabolite repression (CCR; Fernandez *et al*., 2012),

a process ensuring genes for alternative carbon source utilization are repressed when the preferred carbon source glucose is sensed (as G6P) by Tps1. Thus, Tps1 integrates carbon metabolism (via control of CCR) and nitrogen metabolism (via control of Nut1) in response to available G6P. The importance of this carbon-nitrogen metabolic coupling to plant infection is twofold: G6P monitoring allows *M. oryzae* to respond appropriately to available nutrient quantity and quality during infectious growth (Fernandez and Wilson, 2012; Fernandez *et al*., 2012); and the connection between G6P availability, NADPH production and gene expression fuels NADPH-dependent antioxidation systems involving glutathione and thioredoxin that are required for *in planta* colonization (Fernandez and Wilson, 2014b).

Determining what additional regulators – and the processes they control – play key roles in the *M. oryzae* infection cycle would help to build knowledge towards a more comprehensive and mechanistic understanding of fungal crop diseases. To this end, we sought to identify and characterize previously unknown mediators of rice infection, and focused on the sirtuins as candidate regulators for blast disease. Sirtuins are a conserved protein family, found in eukaryotes and prokaryotes (Frye, 2000) but not functionally described in fungal plant pathogens, whose founding member, the *Saccharomyces cerevisiae* protein Sir2 (Rine *et al*., 1979), acts as an NAD-dependent histone deacetylase (Kaeberlein *et al*., 1999; Imai *et al*., 2000; Blander and Guarente, 2004). Histone deacetylases (HDACs) remove acetyl groups from the ε-amino group of lysine residues on histones proteins, thereby affecting chromatin structure and regulating gene expression (Imai *et al*., 2000; Yang and Seto, 2007). HDAC targets can also be non-histone proteins such as transcription factors and metabolic enzymes (Kim *et al*., 2006; Yang and Grégoire, 2007; Yang and Seto, 2007). HDACs are grouped into four classes that are subdivided into two families: classical and sirtuin. Classical HDACs share sequence similarity, often form large multiprotein complexes (Yang and Seto, 2007) and require zinc as a cofactor, whereas the sirtuin family share no sequence similarity to classical members and require NAD^+ as a cofactor (Gregoretti *et al*., 2004). Sirtuins deacetylate substrates such as lysines 9 and 14 of histone H3 and lysine 16 of histone H4 (Imai *et al*., 2000) by using NAD^+ in an ADP-ribosylation reaction distinct from classical HDACs (Blander and Guarente, 2004). During sirtuin deacetylation, NAD^+ is cleaved when an acetyl group from a lysine substrate is transferred to the ADP-ribose moiety of NAD^+, generating nicotinamide and 1-O-acetyl-ADPribose (Imai *et al*., 2000; Tanner *et al*., 2000). The dependence of sirtuins on NAD^+ suggests, like Tps1 in *M. oryzae* (Wilson *et al*., 2010), that their enzymatic activity is linked to the energy and redox status of the cell (Schwer and Verdin, 2008).

Sirtuins have been extensively studied in mammalian systems. Humans and mice possess seven sirtuins (SIRT1–7) (Houtkooper *et al*., 2012). SIRT1–3, 5, 6 exhibit deacetylase activity (Schwer and Verdin, 2008; Finkel *et al*., 2009),

and non-histone deacetylation targets for some sirtuins have been described (Haigis and Sinclair, 2010; Houtkooper *et al*., 2012). Sirtuins have roles in diverse biological and cellular processes including metabolic regulation, homeostasis and nutrient adaptation; transcription factor regulation; apoptosis; and oxidative stress (Haigis and Guarente, 2006; Schwer and Verdin, 2008; Finkel *et al*., 2009; Haigis and Sinclair, 2010; Houtkooper *et al*., 2012; Webster *et al*., 2012; Bause and Haigis, 2013; Wang *et al*., 2014). Sirtuins are important in stress resistance and redox homeostasis: the Sir2/SIRT1 homologue in *Caenorhabditis elegans*, *sir2.1*, is activated by oxidative damage (Wang and Tissenbaum, 2006), while SIRT1 activates the FOXO3 transcription factor in response to oxidative stress to regulate, among other genes, the expression of the antioxidant superoxide dismutase (SOD) (Kops *et al*., 2002; Webster *et al*., 2012). SOD enzymes catalyze the conversion of superoxide (O_2^-) into hydrogen peroxide and oxygen to provide cellular protection against high levels of ROS. Therefore, sirtuins function across taxa to integrate responses to cellular insults such as oxidative stress.

Classical HDACs and their interacting partners have been characterized for roles in plant pathogenicity in a few pathosystems. In the maize pathogen *Cochliobolus carbonum*, the class II HDAC-encoding orthologue of yeast *HOS2*, *HDC1*, was found to be required for virulence (Baidyaroy *et al*., 2001). In *Fusarium graminearum*, the cause of head blight in wheat and barley, the *HOS2* orthologue *HDF1* was required for virulence on wheat heads and corn stalks (Li *et al*., 2011). Also in *F. graminearum*, the product of the transducin beta-like gene *FTL1*, the orthologue of the *S. cerevisiae SIF2* gene, acts in a complex with Hdf1 and is essential for colonizing wheat tissues (Ding *et al*., 2009). The *SIF2* orthologue in *M. oryzae*, *TIG1*, is essential for invasive growth and lesion development and is required for resistance to oxidative stress and plant defense proteins (Ding *et al*., 2010). Tig1 acts in a conserved protein complex with the class II HDAC Hos2, and loss of Hos2 function also prevents rice blast disease (Ding *et al*., 2010).

In contrast to class II HDACs, the roles of class III sirtuin HDACs in plant-fungal interactions have not been described. Therefore, we sought to determine if (and how) putative sirtuin orthologues in *M. oryzae* might contribute to infection-related development and/or pathogenicity during rice infection. Here, we show that the *M. oryzae* sirtuin MoSir2 is essential for rice blast disease. MoSir2 is dispensable for appressorium development and rice cuticle penetration but is essential for biotrophic growth in rice cells due to its role in neutralizing host ROS. To account for this role, we provide evidence that MoSir2 regulates early rice cell infection events by a novel mechanism that does not involve histone deacetylation but instead requires the MoSir2-dependent inactivation of a cupin-like JmjC domain-containing protein that otherwise represses the expression of the superoxide dismutase-encoding gene *MoSOD1* by binding its promoter. When taken together, our

results indicate that, during the early stages of *in planta* growth, MoSir2 deacetylates MoJmjC to alleviate *MoSOD1* transcript repression and detoxify host ROS. This work thus extends our knowledge of how rice blast disease is regulated.

Results

MoSir2 is required for fungal pathogenesis

We targeted the Sir2 family member-encoding gene MGG_10267 (Dean *et al*., 2005), which we have designated *MoSIR2*, for deletion from the genome of the *M. oryzae* wild-type strain Guy11 (Fig. 1A). The resulting Δ*sir2* deletion strains were morphologically similar to Guy11 strains following growth on complete media (CM), and formed normal appressoria on artificial hydrophobic surfaces (Fig. 1B). Δ*sir2* conidiation rates on CM were not significantly different (Student's *t*-test $P > 0.05$) to those of Guy11 strains (Fig. 1C). Moreover, Δ*sir2* radial growth rates on defined minimal media containing 1% glucose as the sole carbon source (1% GMM) (Fig. 1D), in addition to appressorium formation rates on hydrophobic surfaces (Fig. 1E), were not significantly different (Student's *t*-test $P > 0.05$) to Guy11. However, when applied to whole leaves of the susceptible rice cultivar CO-39, Δ*sir2* mutant strains, compared to the pathogenic Guy11 and Δ*sir2 MoSIR2* complementation strains, were unable to develop visible necrotic lesions (Fig. 2A).

To understand why Δ*sir2* strains were non-pathogenic, we first determined that this was not due to impaired or reduced appressorium formation by Δ*sir2* strains on rice leaves (Fig. 2B), or the rate at which Δ*sir2* strains penetrated rice cuticles (Fig. 2C), compared to Guy11. Furthermore, live-cell imaging of detached rice leaf sheaths showed that following penetration, Δ*sir2* strains, like Guy11, could elaborate invasive hyphae (IH) in epidermal cells (Fig. 2D). However, Δ*sir2* growth *in planta* was accompanied by granular depositions not observed in cells infected with Guy11 or Δ*sir2 MoSIR2* complementation strains (Fig. 2D). In addition, the average growth rate of Δ*sir2* strains in rice cells was significantly reduced (Student's *t*-test $P \leq 0.05$) compared to Guy11 at 48 h post inoculation (hpi) (Fig. 2E). Notably, Δ*sir2* growth rates scored less than 4, indicating Δ*sir2* was not observed moving into adjacent cells at 48 hpi (Fig. 2E). Further support for reduced Δ*sir2 in planta* growth is shown in Fig. 2F, where the mass of Δ*sir2* strains in rice cells at 72 hpi was 46-fold less than Guy11, as determined by quantifying the relative amount of fungal DNA in infected leaf tissue. Taken together, these results suggest that MoSir2 is not required for appressorium development or penetrating the host cuticle but is essential for fungal proliferation inside the rice cell.

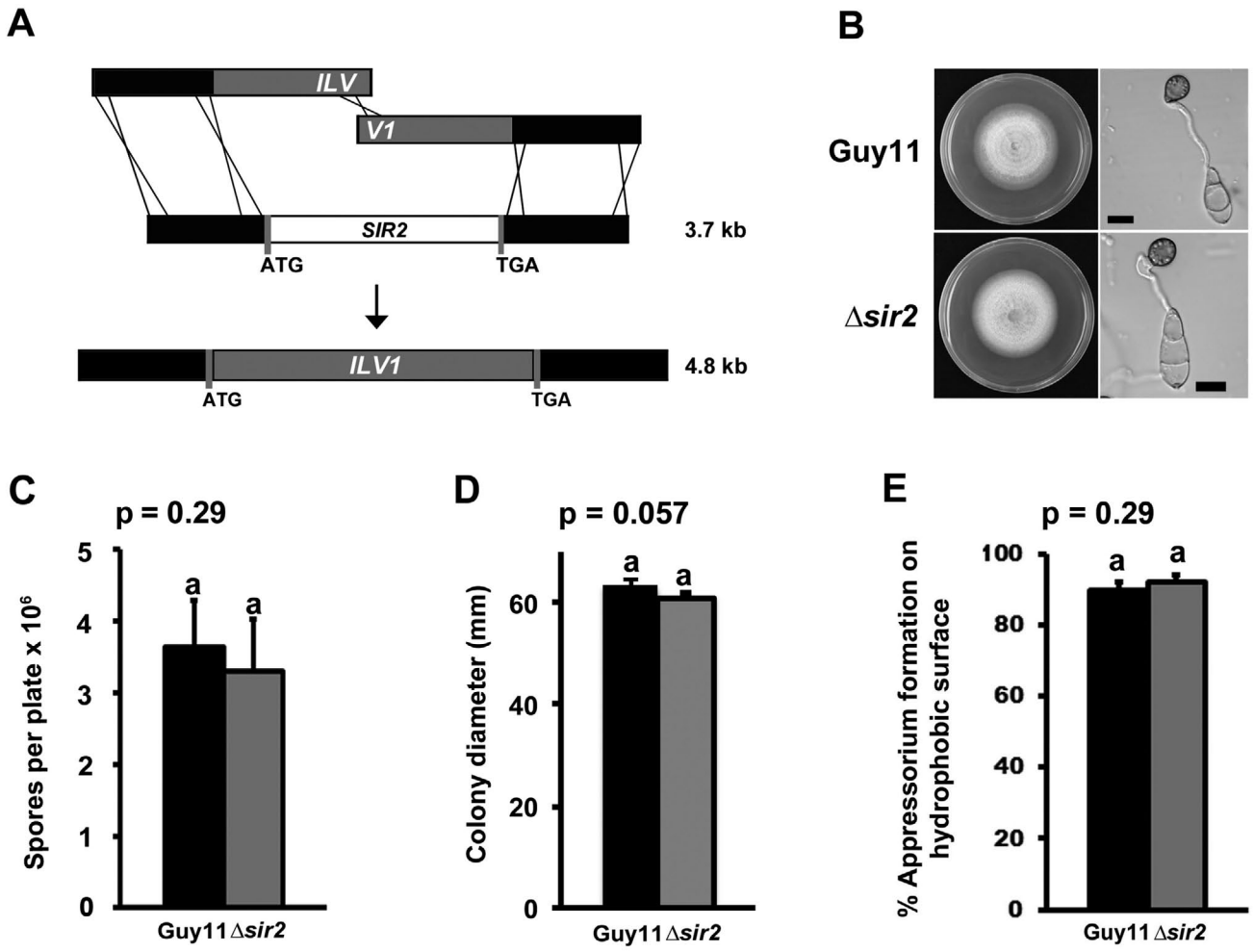

Fig. 1. Functional characterization of MoSir2.

A. A high-throughput, PCR-based split marker deletion strategy (Wilson *et al*., 2010) was employed to replace the 1.7 kb coding sequence of *MoSIR2* with the 2.8 kb *ILV1* gene conferring sulphonylurea resistance.

B. Δ*sir2* colony morphology on complete media was not altered compared to Guy11 parental strains, and spores produced normal looking appressoria on artificial hydrophobic surfaces. Scale bar = 10 μm. C–E. Values are the mean of three independent replicates. Error bars are SD. Bars with the same letter are not significantly different (Student's *t*-test $P > 0.05$).

C. Δ*sir2* strains were not affected in conidiation on complete media (CM) after 12 days growth compared to parental Guy11 strains.

D. Radial growth on defined minimal media, with 1% (w/v) glucose (1% GMM) and 10 mM nitrate as the sole carbon and nitrogen sources, was not affected in Δ*sir2* strains compared to Guy11. Colony diameters were measured at 10 days post inoculation.

E. Δ*sir2* conidia formed appressoria on artificial hydrophobic surfaces at the same rate as Guy11.

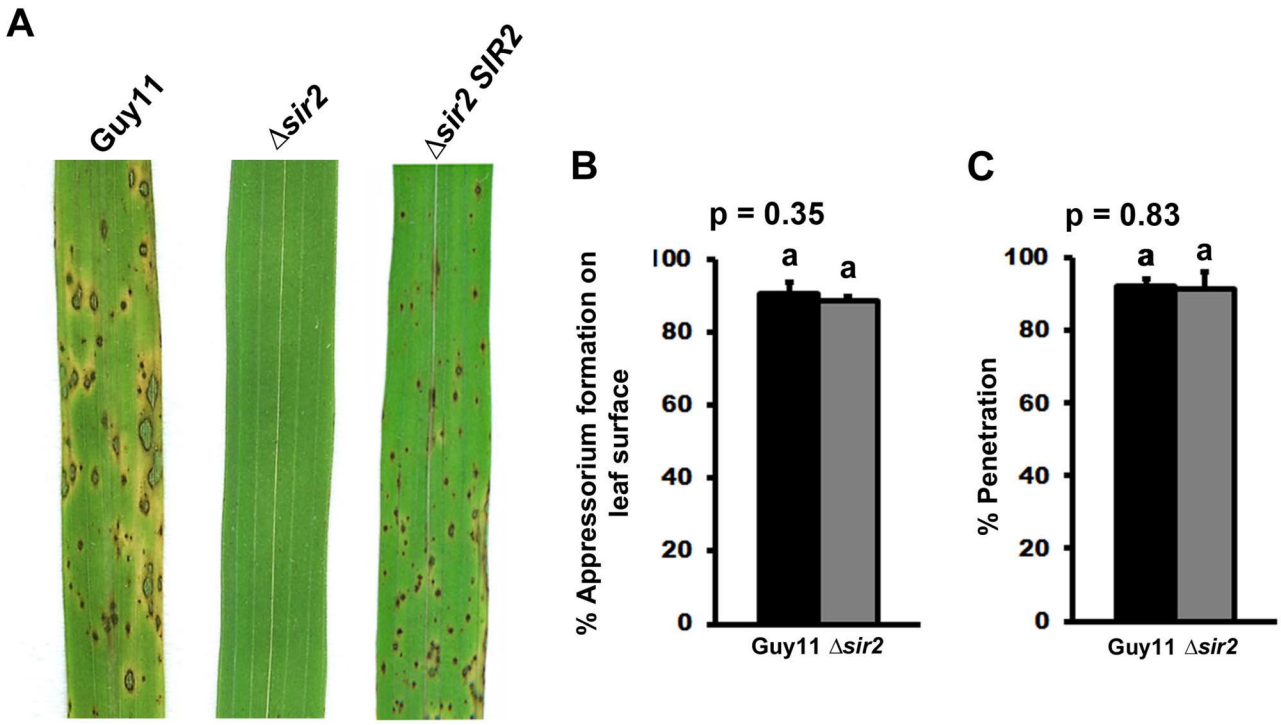

Fig. 2. MoSir2 is essential for pathogenicity.

A. Spores of Δ*sir2* strains were applied to 3-week-old plants of the susceptible cultivar CO-39 at a rate of 5×10^4 spores ml^{-1}. Compared to Guy11 and the Δ*sir2 MoSIR2* complementation strain, Δ*sir2* strains were abolished for pathogenicity. Images were taken at 144 h post inoculation (hpi).

B & C. (B) The rate of appressorial formation by Δ*sir2* strains was not significantly different from Guy11 on rice leaf surfaces at 24 hpi, and (C) the rate of rice leaf penetration by Δ*sir2* strains, determined at 30 hpi, was equivalent to Guy11. Values are the mean of three independent replicates. Each replicate involved counting the number of appressoria formed from 50 conidia (B) or counting how many of 50 appressoria produced a penetration event (C). Error bars are SD. Bars with the same letter are not significantly different (Student's *t*-test $P > 0.05$).

(Continued)

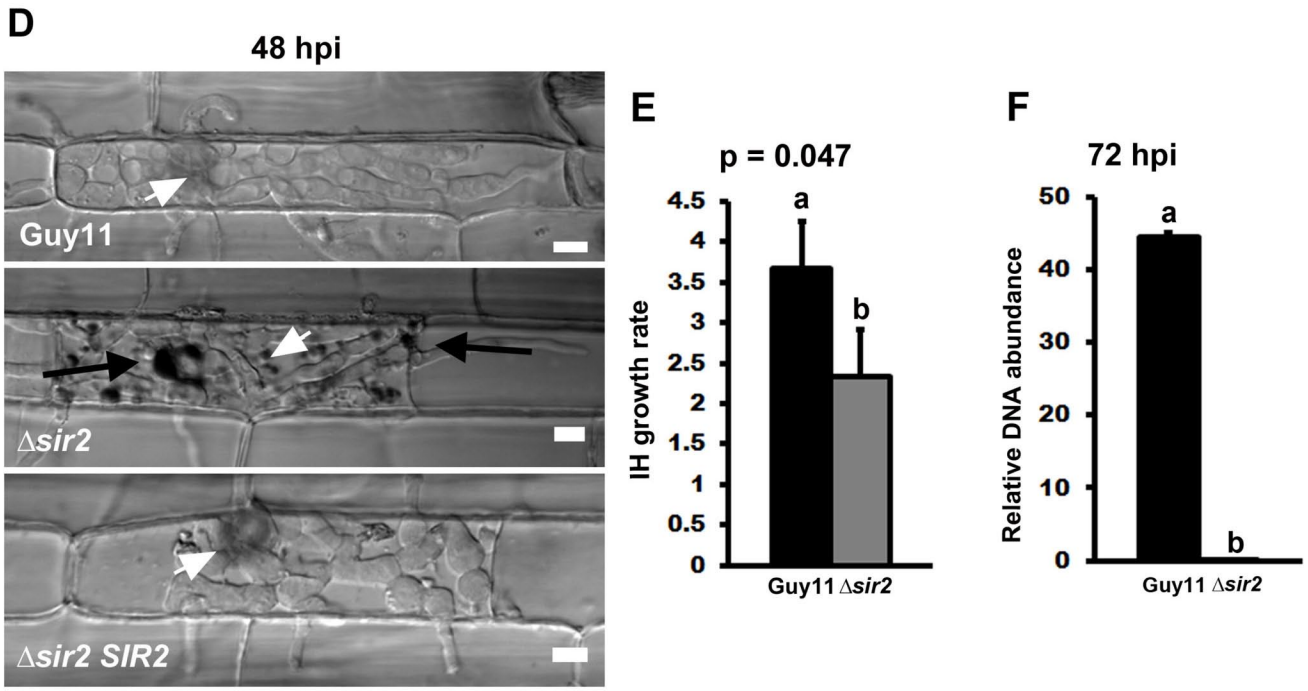

Fig. 2. (continued) MoSir2 is essential for pathogenicity.

D. Live-cell imaging at 48 hpi of Guy11, Δ*sir2* and Δ*sir2 MoSIR2* complementation strains infecting susceptible CO-39 detached rice leaf sheaths. Rice cell infection by Δ*sir2* promoted the formation of granules inside the primary infected rice cell. Scale bar is 5 μm. White arrowheads indicate appressoria on the surface of the leaf and the penetration site, and black arrowheads indicate examples of the granules observed inside Δ*sir2* infected rice cells.

E. The growth rate of Δ*sir2* and Guy11 invasive hyphae (IH) was determined at 48 hpi. Values are the mean of three independent replicates. Each replicate involved measuring the growth rate in 50 infected cells. Bars with different letters are significantly different (Student's *t*-test $P \leq 0.05$). Error bars denote SD. The growth rate of IH was measured using a 1–4 scale described by Wilson and associates (Wilson *et al*., 2012), where 1 = IH length shorter than 10 μm with no branching; 2 = IH length is 10–20 μm with 0–2 branches; 3 = IH length is longer than 20 μm and/or with more than 2 branches within one cell; 4 = IH has spread to adjacent cells.

F. At 72 hpi, leaves infected with Guy11 were found to contain 46-fold more fungal DNA than leaves infected with Δ*sir2* strains. Values are given as the average of three independent measurements of *MoACT1* normalized against rice actin, using total DNA isolated from rice leaves as a template. Bars with different letters are significantly different (Student's *t*-test $P \leq 0.05$). Error bars denote SD.

MoSir2 is required for neutralizing ROS under axenic growth conditions

We wondered why IH proliferation was impaired in Δ*sir2* strains. First, considering the classic role of sirtuins in calorie restriction (Finkel *et al*., 2009), we sought to determine how Δ*sir2* strains grew on media with low concentrations of glucose. Figure 2A shows that Δ*sir2* strains were not impaired in axenic growth on GMM plates containing reduced concentrations of glucose (< 1% w/v) compared to Guy11. Rather, growth of Δ*sir2*, relative to Guy11, was impaired on media containing elevated concentrations of glucose (> 1% w/v). In contrast, the Δ*sir2 SIR2* complement strains grew like Guy11 on 20% GMM (Fig. S1). Thus, MoSir2 is required for glucose tolerance at high concentrations.

In addition to poor growth on high levels of glucose, stress tests revealed Δ*sir2* strains were more susceptible than Guy11 to the oxidant hydrogen peroxide (Fig. 3B), but were not affected by the cell wall disruptant Congo Red or the osmotic stressors NaCl and sorbitol (Fig. S2). These results suggest that MoSir2 does not play a general role in cellular stress responses but might instead be specifically required for adaptation to oxidative insults.

How is the role of MoSir2 in neutralizing oxidative stress related to its role in glucose tolerance? In mammalian endothelial cells, exposure to high glucose concentrations can affect redox balance and increase ROS production (Zhang *et al*., 2012). Figure 3C shows that a similar process might occur in *M. oryzae* because treating 10% GMM with diphenyleneiodonium (DPI), an inhibitor of NADPH oxidases (Chi *et al*., 2009), restored the growth of Δ*sir2* strains compared to Guy11. Thus, the requirement for MoSir2 during growth on high levels of glucose might stem from a role for this protein in ROS quenching.

To understand more about the role of MoSir2 in glucose tolerance, we next sought to understand how *MoSIR2* gene expression was regulated. *MoSIR2* expression levels were not significantly different (Student's *t*-test $P > 0.05$) following the growth of Guy11 on 10% GMM compared to 1%GMM(data not shown). However, MoSir2 activity might be fine-tuned in response to glucose levels by the sugar sensor Tps1 because *MoSIR2* expression was elevated in Δ*tps1* strains on 1% GMM compared to Guy11 (Fig. S3). Because Tps1 is required for CCR in the presence of glucose (Fernandez *et al*., 2012), this suggests Tps1 could repress *MoSIR2* expression under optimal (i.e. 1% glucose) growth conditions. Conversely, Δ*tps1* strains were not attenuated for growth on 10% and 20%GMMwith ammonium as the sole nitrogen source compared to Δ*sir2* strains (data not shown), indicating Tps1 is not required for MoSir2 activity under suboptimal glucose conditions.

In response to fungal invasion, rice cells produce ROS that must be neutralized by the pathogen for a compatible reaction to take place (Chi *et al*.,

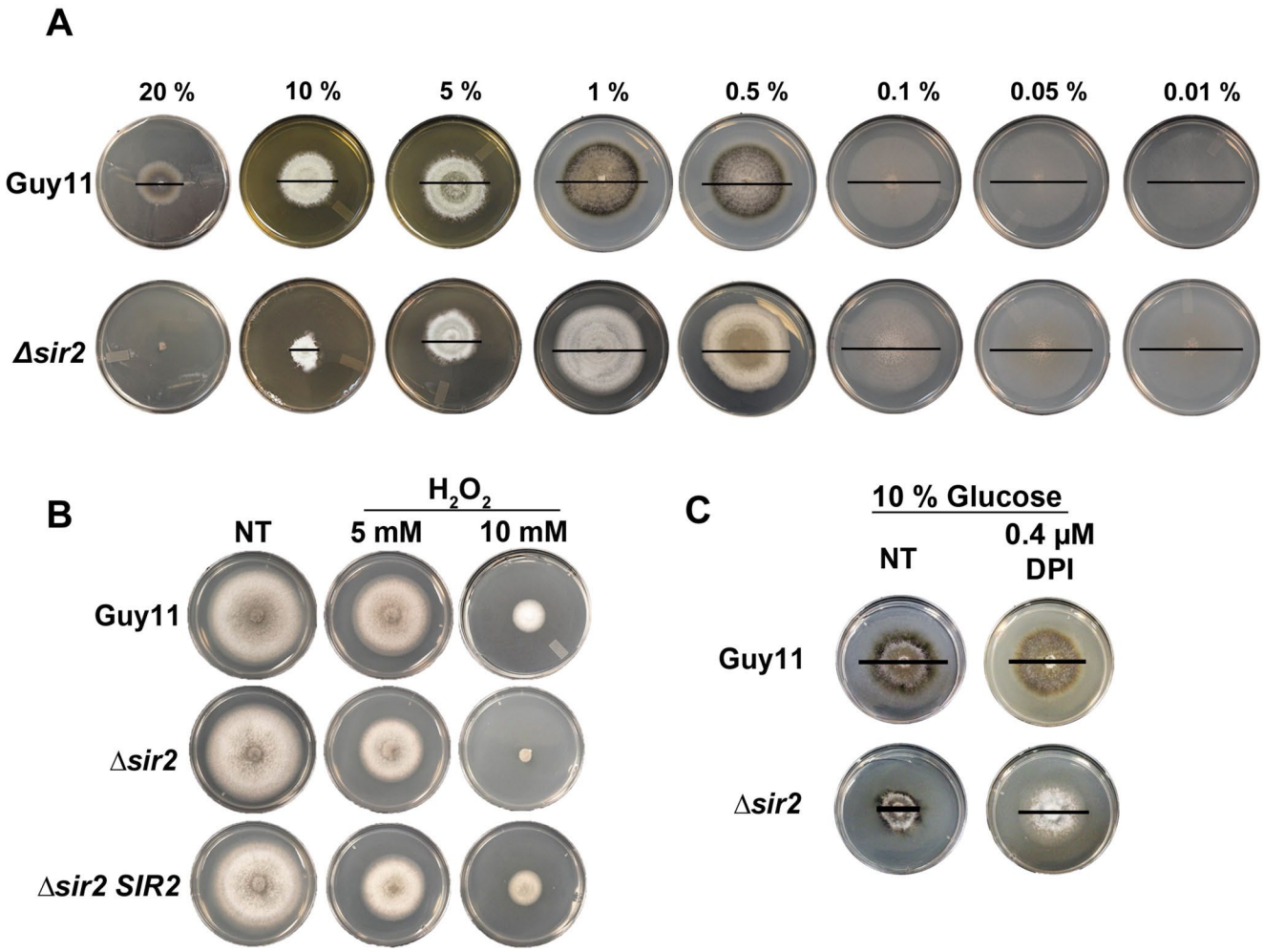

Fig. 3. MoSir2 is required for glucose tolerance and resistance to oxidative stress.

A. Strains of Guy11 and Δ*sir2* were inoculated as 10 mm mycelial plugs onto 85 mm diameter plates of minimal media (MM) with 10 mM nitrate as the nitrogen source and containing increasing concentrations (w/v) of glucose, indicated above each plate. Plates were imaged after 10 days. Colony diameters are indicated with black bar for ease of viewing.

B. Strains were grown on 55 mm diameter plates of CM containing H_2O_2 at the concentrations indicated. Images were taken after 5 days. NT, no treatment.

C. For best results, strains were grown on 55 mm diameter plates of 10% GMM containing the NADPH oxidase inhibitor diphenyleneiodonium (DPI) at the concentration indicated. Images were taken after 10 days. NT, no treatment.

2009; Huang *et al*., 2011; Fernandez and Wilson, 2014b). We tested whether Δ*sir2* strains were impaired in neutralizing oxidative stresses *in planta* by staining detached leaf sheaths infected with Guy11 or Δ*sir2* strains with 3,3′-diaminobenzidine (DAB). Rice cells infected with Δ*sir2* strains stained strongly and produced an orange pigment when incubated with DAB (Fig. 4A), indicating the accumulation of hydrogen peroxide (H_2O_2) at infection

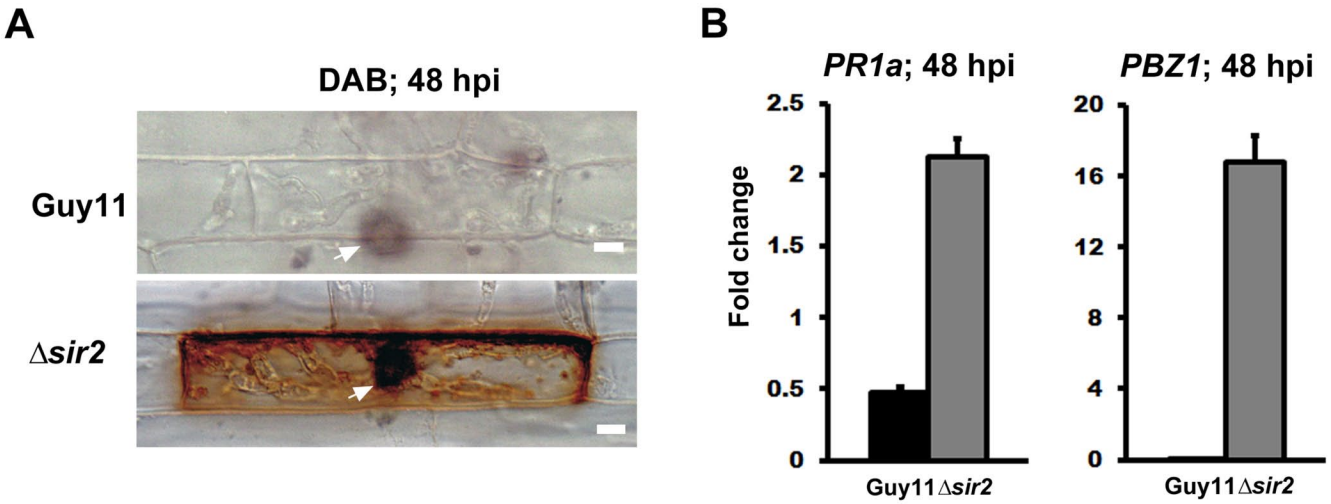

Fig. 4. MoSir2 is required for suppressing plant defenses.

A. Rice sheaths inoculated with Δ*sir2* strains showed strong DAB staining at 48 hpi indicative of H2O2 accumulation at penetration sites. No staining was observed for cells infected with Guy11. Rice sheaths were inoculated with 5×10^4 conidia ml^{-1} of each strain. Samples were observed at 48 hpi. Arrowheads indicate the appressoria on the rice sheath surface. Bar = 5 μm.

B. The expression of *PR1a* and *PBZ1* was analyzed in rice cells infected with Guy11 and Δ*sir2* strains at 48 hpi. Fold changes in gene expression are calculated from the average of three independent measurements, normalized against *M. oryzae* actin gene expression. Error bars are SD.

sites and confirming that Δ*sir2* strains are impaired for ROS neutralization *in planta*. ROS accumulation can elicit robust plant defense responses including granule generation in rice cells and the expression of rice pathogenesis-related (PR) genes (Chi *et al*., 2009). We isolated RNA from detached rice leaf sheaths infected with Guy11 and Δ*sir2* strains and used quantitative real-time PCR (qRT-PCR) to analyze the expression levels of two rice PR genes, *PR1a* and *PBZ1* (Chi *et al*., 2009). Figure 4B shows that PR gene expression was elevated in leaf sheaths infected with Δ*sir2* but not Guy11 strains, suggesting enhanced plant defense responses occur in rice cells challenged with Δ*sir2*.

Elevated plant defense responses resulting from impaired ROS neutralization by Δ*sir2* strains might also account for the granular depositions observed in Δ*sir2* infected rice cells (Chi *et al*., 2009) (Fig. 1E). Consistent with this, we found that treating Δ*sir2* spores with the NADPH oxidase inhibitor DPI before applying to detached rice leaf sheaths prevented granular accumulation in rice cells (Fig. 5A). The concentration of DPI used in this experiment did not inhibit appressorium formation on the host leaf surface (Fig. 5B), but was sufficient to permit Δ*sir2* strains to spread into adjacent cells from primary infected cells (Fig. 5C). Untreated Δ*sir2* strains could not move

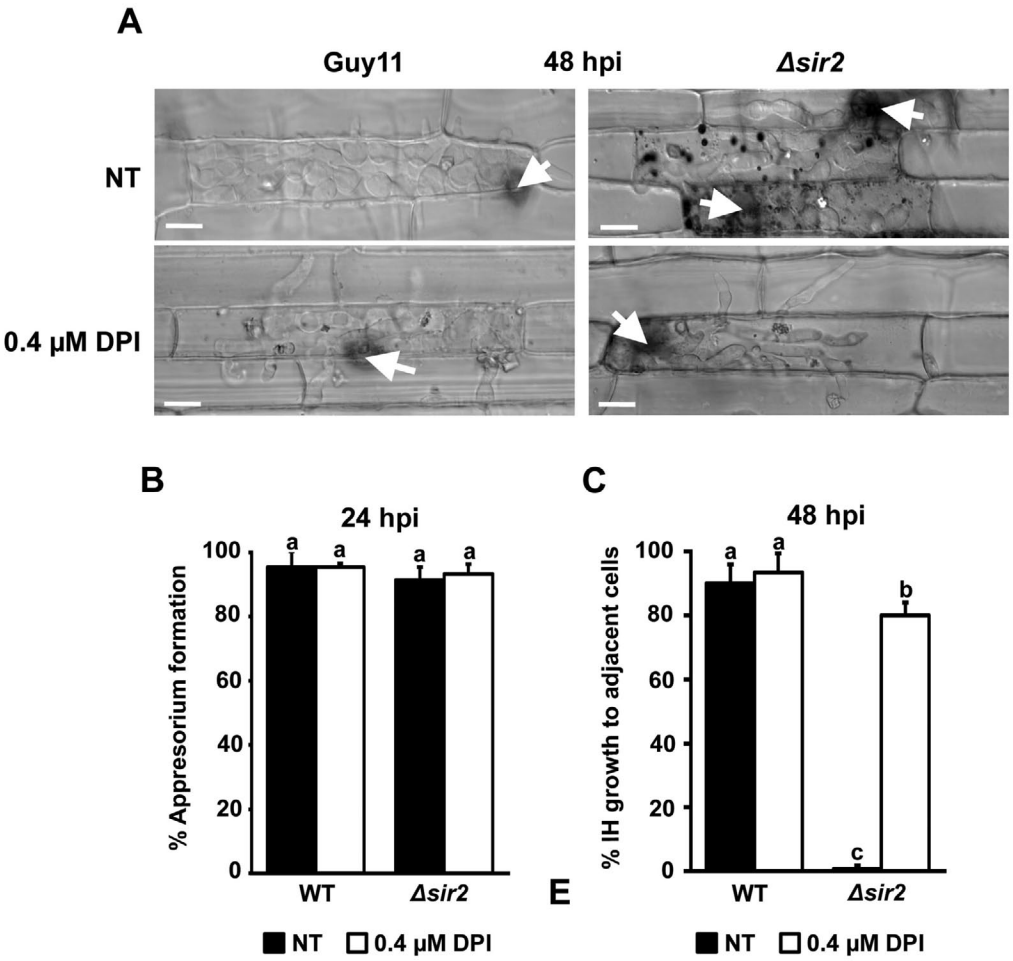

Fig. 5. Inoculating rice leaf sheaths with Δ*sir2* spores treated with DPI suppressed plant responses and promoted *in planta* growth.

A. Rice sheaths were inoculated with 5×10^4 conidia ml^{-1} of Δ*sir2* and Guy11 strains. Compared to no treatment (NT), Δ*sir2* strains treated with DPI at the indicated concentration did not elicit a plant response and granule formation was not observed at 48 hpi. Arrowheads indicate appressoria on the rice sheath surface. Bar = 5 μm.

B. DPI treatment at the indicated concentration did not affect appressorium formation on rice leaf sheaths at 24 hpi compared to no treatment (NT). Values are the mean of three independent replicates. Error bars are SD. Bars with the same letter are not significantly different (Student's *t*-test $P > 0.05$).

C. Cell-to-cell growth of Δ*sir2* IH was significantly improved following DPI treatment compared to no treatment (NT). Values are the mean of three independent replicates. Each replicate involved measuring how many of 50 penetration sites resulted in IH moving to adjacent cells by 48 hpi. Bars with different letters are significantly different (Student's *t*-test $P \leq 0.05$). Error bars denote SD.

to adjacent cells. Taken together, the results presented here demonstrate that MoSir2 is required for neutralizing host-derived ROS and suppressing rice defense responses to facilitate at least the early stages of rice cell infection.

MoSod1 is an output of MoSir2 signaling

To gain a deeper understanding of the role of MoSir2 in rice infection, we next sought to identify what cellular processes might be under MoSir2 control. To achieve this, we exploited the reduced ability of Δ*sir2* strains to grow on elevated glucose concentrations (due to impaired ROS neutralization) to perform a comparative proteome analysis of this mutant against Guy11. Strains of Guy11 and Δ*sir2* were grown in liquid shake minimal media containing 1% or 10% glucose and total cell proteins were extracted and analyzed by LC-MS/MS (Table S1). Table 1 shows the identity and relative quantity of proteins more abundant in either Guy11 or Δ*sir2* samples following growth in 10% GMM. Consistent with increased sensitivity of Δ*sir2* strains to both ROS and high glucose concentrations, we were interested to note that one of the proteins highly expressed in Guy11 strains on 10% glucose, but not detected in Δ*sir2*, was a putative superoxide dismutase encoded by MGG_02625 (Dean *et al*., 2005), a homologue of yeast and human *SOD1*. Like yeast Sod1 (Outten *et al*., 2005), MoSod1 is cofactored with Cu/Zn and PSORTII analysis predicts it is located in the cytoplasm.

To confirm MoSod1 acts downstream of MoSir2, we deleted the *MoSOD1* gene from the genome of Guy11. The resulting Δ*sod1* strain, like both the *M. oryzae* Δ*sir2* strain (Fig. 3B) and the yeast Δ*sod1* strain (Outten *et al*., 2005), was sensitive to H_2O_2 and, like the *M. oryzae* Δ*sir2* strain (Fig. 3A), was restricted in growth on 10% GMM compared to Guy11 (Fig. 6A). Like Δ*sir2* strains, Δ*sod1* strains also elicited strong plant defense responses in infected

Table 1. Relative abundance of identified proteins from mycelia of Guy11 compared to Δ*sir2* strains following growth on 10% GMM.

		Quantitative value	
Allele	*Identified proteins*	*Guy11 10% Glucose*	*Δsir2 10% Glucose*
MGG_02625	Superoxide dismutase	17	0
MGG_06958	hsp70-like protein	11	3
MGG_06135	GTP-binding protein SAS1	9	0
MGG_05673	40S ribosomal protein S3	9	0
MGG_15113	Pyridoxal reductase	8	0
MGG_04913	Conserved hypothetical protein	3	42
MGG_01084	Glyceraldehyde-3-phosphate dehydrogenase	3	21
MGG_02386	Autophagy protein Atg27	0	20
MGG_06185	Hypothetical protein	2	14
MGG_08622	Nucleoside diphosphate kinase	0	16
MGG_10607	Enolase	0	14
MGG_00445	Cupin-like JmjC domain-containing protein	0	8
MGG_00806	Polyketide synthase	0	8

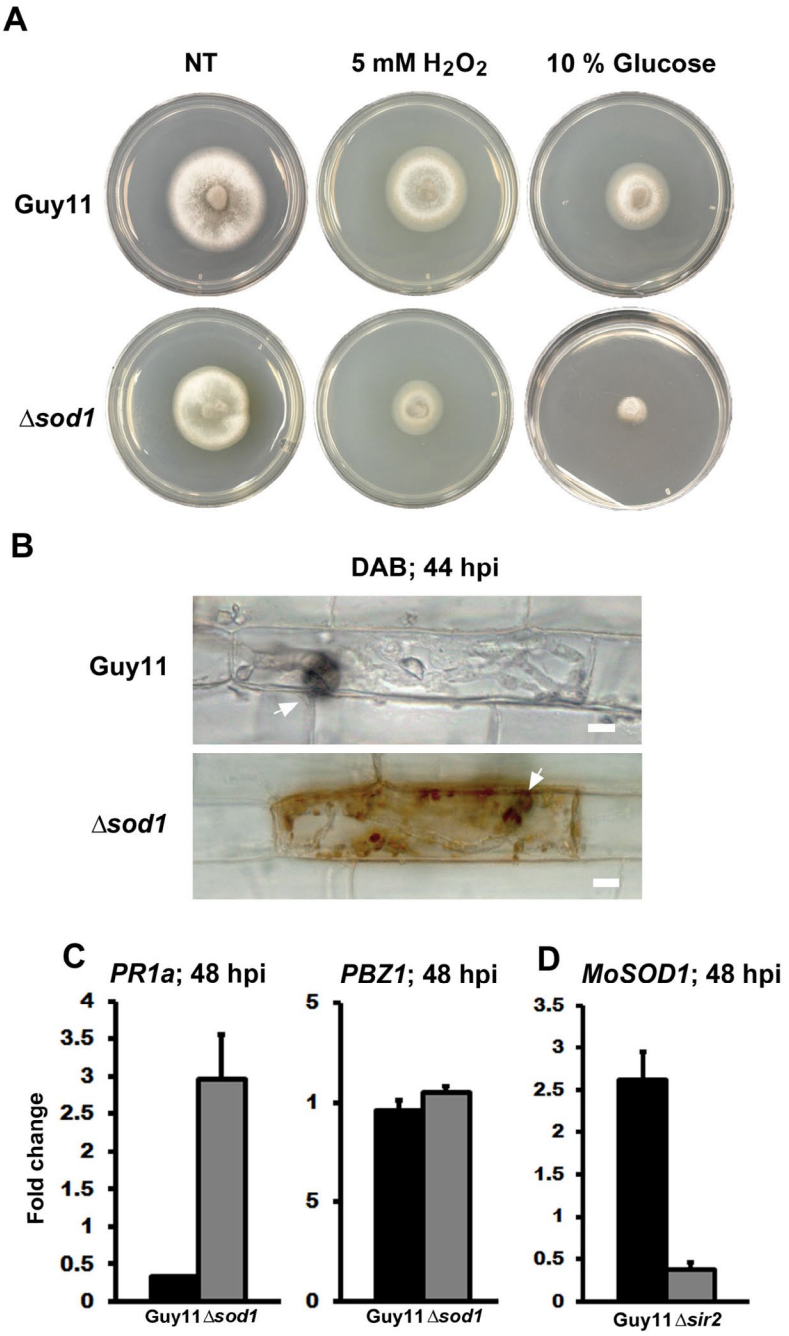

Fig. 6. MoSod1 is an output for MoSir2.

A. Strains of Guy11 and Δ*sod1* were inoculated as mycelial plugs onto 55 mm diameter plates of CM, with and without 5 mM H_2O_2, and onto MM with 10% glucose. Images were taken after 5 days. NT, no treatment.

B. Δ*sod1* elicited H_2O_2 accumulation in infected rice cells as evidenced by increased DAB staining compared to Guy11. Samples were observed at 44 hpi. Arrowheads indicate the appressoria on the rice sheath surface. Bar = 5 µm.

C & D. Fold changes in gene expression are calculated from the average of three independent measurements, normalized against *M. oryzae* actin gene expression. Error bars are SD. (C) PR gene expression was altered at 48 hpi in rice cells infected with Δ*sod1* strains compared to Guy11. (D) MoSir2 is required for the maximum expression of *MoSOD1* during *in planta* colonization, and the expression of *MoSOD1* was downregulated in Δ*sir2* compared to Guy11 at 48 hpi.

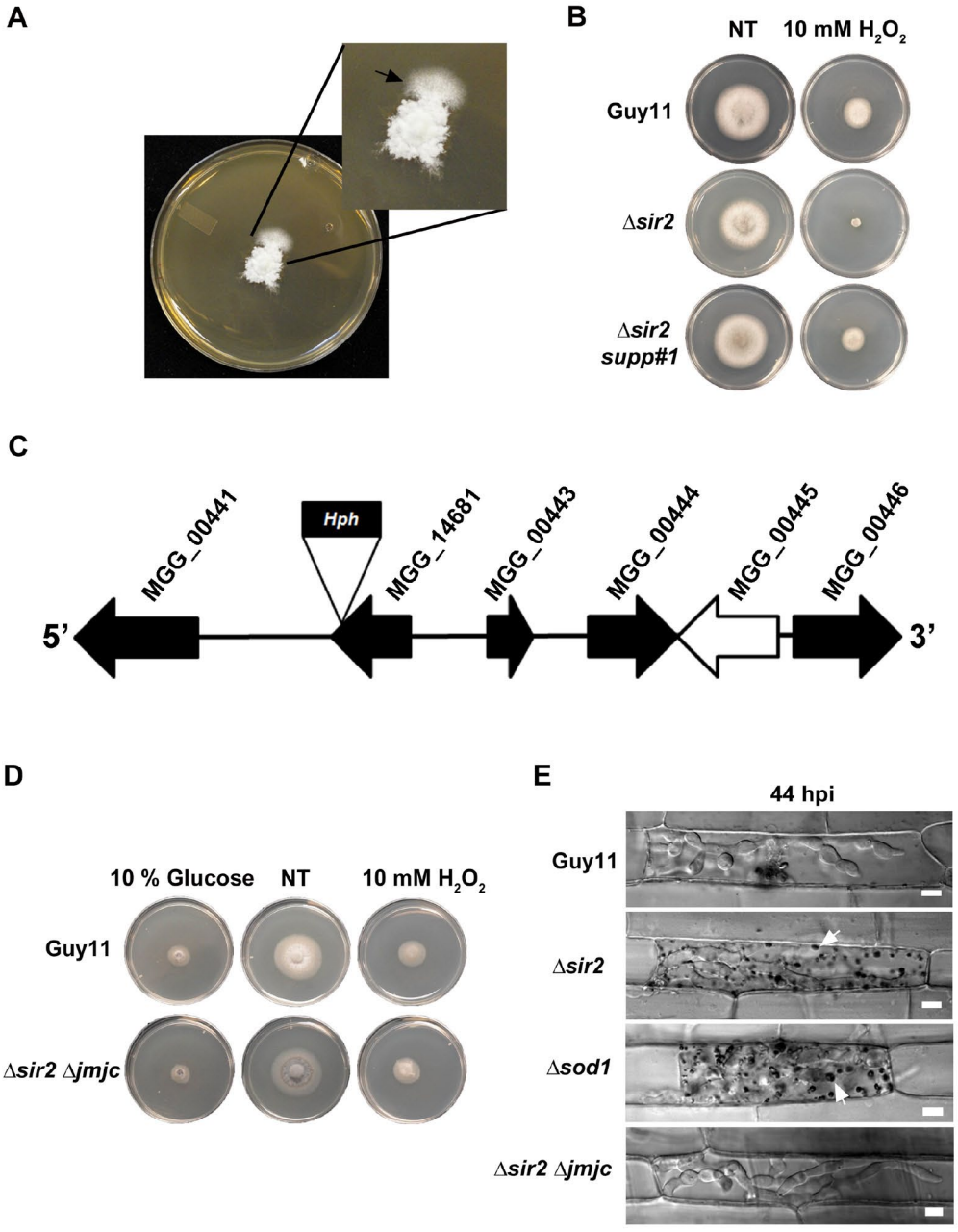

Fig. 7. Identifying and characterizing an extragenic suppressor of Δ*sir2*.

A. A spontaneous suppressor of Δ*sir2* (arrowhead) emerged from a Δ*sir2* colony grown for 15 days on 10% GMM.

B. The Δ*sir2 supp#1* suppressor was resistant to H_2O_2 compared to Δ*sir2* parental strains. Images were taken after 5 days growth on CM. NT, CM with no treatment.

C. Genomic location of T-DNA insertion resulting in the extragenic suppressor strain Δ*sir2 AT-Supp 7*. TAIL-PCR was used to identify the location of the *Hph* gene inserted by ATMT and resulting in the generation of the Δ*sir2* extragenic suppressor strain, Δ*sir2 AT-Supp 7*, restored for growth on 10% GMM.

D. Δ*sir2* Δ*jmjc* double mutant strains grew indistinguishably from Guy11 on 10% GMM and on CM containing 10 mM H2O2. NT, CM with no treatment.

E. Δ*sir2* Δ*jmjc* strains did not elicit granule deposition (white arrowheads) in rice cells at 44 hpi. Bar: 5 µm

rice epidermal cells including H_2O_2 accumulation revealed by DAB staining (Fig. 6B), granular depositions (Figs 6B and 7E) and elevated expression of the PR gene *PR1a* (but not *PBZ1*, see below) (Fig. 6C). Therefore, Δ*sod1* strains mimic Δ*sir2* strains on axenic plate tests and in rice epidermal cells, indicating MoSod1 regulation is an output of MoSir2.

MoSod1 is regulated by MoSir2 at the transcript level

To gain insights into how MoSir2 might regulate MoSod1 accumulation in Guy11 (Table 1), we next sought to determine whether MoSod1 was a direct target for MoSir2 and therefore regulated at the protein level, or regulated indirectly by MoSod1 at the transcript level. Although unrelated to SOD1, mammalian mitochondrial SOD2 is a substrate for SIRT3, which modulates its activity by deacetylation (Chen *et al*., 2011). To determine if MoSod1 was similarly a target for deacetylation by MoSir2, we used mass spectrometry to perform a global protein acetylation analysis (Kim *et al*., 2006) on the Guy11 and Δ*sir2* proteome following growth on 1% and 10% GMM (Tables S2 and S3). Table 2 shows the proteins identified in Tables S2 and S3 as being more highly acetylated in Δ*sir2* strains than Guy11 on 10% GMM. Comparing Table 1 with Table 2 shows that some proteins (Atg27, nucleoside diphosphate kinase, enolase, a cupin-like JmjC domain-containing protein and a polyketide synthase), were both more acetylated and more abundant in Δ*sir2* samples grown on 10% GMM compared to Guy11. Acetylated enolase in Δ*sir2* samples is consistent with studies of SIRT3, which have shown it is a deacetylase of metabolic enzymes including glutamate dehydrogenase and isocitrate dehydrogenase and might have a role in gluconeogenesis; and with studies of SIRT2, which stabilizes the gluconeogenic enzyme PEPCK (Lombard *et al*., 2007; Haigis and Sinclair, 2010; Houtkooper *et al*., 2012). Acetylated MoSod1 was not, however, detected under any of the conditions examined. This suggests deacetylated MoSod1 in Guy11 on 10% GMM is the active form of the protein, but we consider it unlikely that inactive MoSod1 is acetylated because if so, it would have been detected in our Δ*sir2* acetylome samples. Therefore, MoSod1 is not likely a direct target for deacetylation by MoSir2. Instead, then, we considered MoSir2 might regulate MoSod1 activity at the transcript level. We therefore studied the expression of *MoSOD1* and found it was downregulated in Δ*sir2* strains on 10% GMM compared to Guy11 (data not shown). Importantly, we also found that *MoSOD1* expression was downregulated *in planta* in Δ*sir2* strains compared to Guy11 (Fig. 6A). This suggests MoSir2 regulates *MoSOD1* gene expression during both *in planta* rice infection and *ex planta* growth on high glucose media.

Table 2. Acetylated proteins identified in the mycelia of Δ*sir2* strains compared to Guy11 following growth in 10% GMM.

		Quantitative value	
Allele	*Identified proteins*	*Guy11 10% Glucose*	*Δsir2 10% Glucose*
MGG_02386	Autophagy protein Atg27	0	15
MGG_04913	Conserved hypothetical protein	0	16
MGG_00445	Cupin-like JmjC domain-containing protein	0	6
MGG_05925	Polyketide synthase	0	6
MGG_08622	Nucleoside diphosphate kinase	0	5
MGG_03549	RAD 54	0	3
MGG_10607	Enolase	0	1

MoSir2 regulates MoSOD2 gene expression in planta

Although MoSod1 is necessary for some MoSir2 functions (Fig. 6A–C), the loss of MoSod1 in Guy11 did not fully recapitulate the Δ*sir2* phenotype. Unlike Δ*sir2* colonization, *PBZ1* expression was not altered in rice cells infected with Δ*sod1* (Fig. 6C), and Δ*sod1* strains remained pathogenic on whole rice leaves (data not shown). These observations limit the action of MoSod1 to the early stages of rice epidermal cell infection and are indicative of a role for other MoSir2-dependent genes during rice cell infection. The *M. oryzae* genome carries a total of three genes encoding putative SODs (Table S4) (Dean *et al*., 2005). The human genome also carries three *SOD* genes: *SOD1* encodes a cytoplasmically located Cu/Zn SOD homologous to MoSod1; *SOD2* encodes a mitochondrial Fe/Mn SOD; and *SOD3* encodes a secreted Cu/Zn SOD (Miao and St Clair, 2009). Table S4 shows that, in addition to *MoSOD1*, the *M. oryzae* genome carries two genes encoding Fe/Mn SODs predicted by PSORTII to be localized to the mitochondrion (MGG_00212) and cytoplasm (MGG_07697). Like yeast, *M. oryzae* does not appear to carry an extracellular Cu/Zn SOD, and SignalP did not detect a signal peptide cleavage site for the SODs in Table S4. However, the genome of *M. oryzae* also carries two genes encoding Cu/Zn-like SODs (MGG_03350 and MGG_13177) that encode larger proteins than MoSod1 and which are not retrieved by BLAST using the *MoSOD1*-coding sequence. They are therefore not likely bona fide SODs and it is unknown if they have SOD activities, thus they were not included in this study. Nonetheless, it is worth noting for future studies that MGG_03550 is predicted by PSORTII to be extracellular localized and by SignalP to carry a signal peptide cleavage site.

We examined the expression of the Fe/Mn SOD encoding genes MGG_00212 and MGG_07697 in Guy11 and Δ*sir2* strains, in rice cells, at 48 hpi (Fig. S4). Guy11 expressed both genes in rice cells and MGG_00212, like *MoSOD1*, was reduced more than twofold in expression in Δ*sir2* strains during rice cell infection compared to Guy11. In contrast, MGG_07697 was slightly downregulated in Δ*sir2* strains compared to Guy11, but the fold change was less than two. Thus, in addition to *MoSOD1*, our transcript data indicate MoSir2 also controls the expression of MGG_00212 – encoding a likely MoSod2 orthologue localized to the mitochondrion – during rice infection. This could account for the phenotypic differences between Δ*sod1* and Δ*sir2* strains during infection.

Whereas *MoSOD1* is one of two MoSir2-dependent SODs expressed *in planta*, the poor growth of Δ*sod1* on 10% GMM (Fig. 6A) is interesting because, in contrast, it suggests only MoSod1 is sufficient for growth on 10% GMM. To account for this observation, we analyzed the expression of the SOD genes in Table S4 following growth on 10% GMM (Fig. S5). *MoSOD1* alone was highly expressed under these growth conditions. Thus, in addition to differences in localization (Table S4), different SODs are not equivalent in their physiological roles and, under at least some growth conditions, how they are expressed.

A JmjC domain-containing protein functions downstream of MoSir2 as a negative regulator of MoSOD1 expression

More mechanistic insights into the action of MoSir2 on downstream processes resulted from a spontaneous suppressor of Δ*sir2* which arose as a sector on a plate of 10% GMM containing a 15-day-old colony of Δ*sir2* (Fig. 7A). This suppressor, named Δ*sir2 supp#1*, was purified on 10% GMM and was resistant to H_2O_2 (Fig. 7B), highlighting the strong link between the ability of *M. oryzae* to tolerate elevated glucose concentrations and its capacity for ROS detoxification.

The remediated growth of Δ*sir2 supp#1* on 10% GMM led us to reason that the requirement for MoSir2 in antioxidation might be by-passed by mutations in genes acting downstream of, or in parallel to, *MoSIR2*. Therefore, we next instigated a forward genetic screen to generate and identify extragenic suppressors of Δ*sir2* that were restored for growth on elevated glucose media by using *Agrobacterium tumefaciens*-mediated transformation (ATMT) to randomly introduce T-DNA containing the hygromycin resistance-conferring gene *Hph* (Fernandez *et al*., 2012) into the Δ*sir2* genome. Extragenic suppressors of Δ*sir2* were dual-selected for hygromycin resistance and growth on minimal media containing 10% or 20% glucose as the sole carbon source. A total of eight strains were initially isolated, of which two Δ*sir2* extragenic suppressor strains, Δ*sir2 AT-Supp 12a* and Δ*sir2 AT-Supp 7*,

remained stable throughout the recovery procedure. Δ*sir2 AT-Supp 12a* was shown by TAIL-PCR (Chen *et al*., 2011) to result from *Hph* gene insertion into MGG_02256 encoding a FAD-binding domain-containing protein. Δ*sir2 AT-Supp 7* was shown to result from *Hph* gene insertion into MGG_14681 encoding a conserved hypothetical protein (Table 3). The low number of extragenic suppressors recovered using ATMT and media selection is consistent with a previous, unrelated study from our group using the same method (Fernandez *et al*., 2012).

Interestingly, MGG_14681 is located near MGG_00445 (Fig. 7C) which encodes the cupin-like JmjC domain-containing protein shown in Tables 1 and 2 to be more abundant and acetylated, respectively, in Δ*sir2* strains grown on 10% GMM compared to Guy11. Thus, MGG_00445, which we have called *MoJMJC*, is functionally connected to MoSir2 at the protein level (Tables 1 and 2). Because T-DNA insertion can affect gene function at distal locations (Tucker *et al*., 2010), we considered that altered *MoJMJC* expression resulting from the downstream insertion of *Hph* (Fig. 7C) might act to suppress the Δ*sir2* antioxidation phenotype in Δ*sir2 AT-Supp 7* strains. Indeed, Fig. S6 shows how the expression of *MoJMJC* is reduced in Δ*sir2 AT-Supp 7* strains, compared to Guy11 and Δ*sir2*, following growth in GMM. Downregulation of *MoJMJC* gene expression could result in suppression of the Δ*sir2* phenotype if, as the proteomic data suggested, MoJmjC was a downstream, negatively acting, component of MoSir2 signaling. On the basis of the proteomic and transcript data, we proceeded to characterize *MoJMJC* as a candidate suppressor of Δ*sir2* with the proviso that the other genes in Fig. 7C, including MGG_14681, would be subsequently analyzed if MoJmjC proved not to be involved in MoSir2 signaling.

To determine if *MoJMJC* was the suppressing allele for Δ*sir2*, we disrupted this gene by targeted homologous recombination in the Δ*sir2* parental strain. The resulting Δ*sir2* Δ*jmjc* double mutant strain, unlike the Δ*sir2* parental strain, was not susceptible to oxidative stress and was indistinguishable from Guy11 during growth on 10% GMM (Fig. 7D). Unlike

Table 3. Δ*sir2* extragenic suppressor strains generated by *Agrobacterium tumefaciens*-mediated mutagenesis (ATMT) and identified by TAIL-PCR.

Selection media	*Parental strain*	*Suppressor strain*	*Locus*	*Protein family*	*Border*	*Length*	*Position of insertion*
20% Glucose	Δ*sir2*	Δ*sir2 AT-Supp 12a*	MGG_02256	FAD-dependent hydroxylase	LB	1356 nt	Upstream of nucleotide 3100303
10% Glucose	Δ*sir2*	Δ*sir2 AT-Supp 7*	MGG_14681	Conserved hypothetical protein	RB	1110 nt	Downstream of nucleotide 2591133

Δ*sir2* or Δ*sod1* strains, the Δ*sir2* Δ*jmjc* double mutant strain was able to colonize rice epidermal cells without eliciting granular depositions (Fig. 7E). In addition, Δ*sir2* Δ*jmjc* double mutant strains were remediated for *MoSOD1* expression, at 48 hpi in rice cells, compared to Δ*sir2* parental strains (Fig. 8A). MGG_00212 expression was not remediated *in planta* at 48 hpi in Δ*sir2* Δ*jmjc* double mutant strains (Fig. S7). Similar to Guy11, but unlike Δ*sir2* and Δ*sod1* strains, the Δ*sir2* Δ*jmjc* double mutant strain did not induce *PR* gene expression at 48 hpi (Fig. 8B). However, the Δ*sir2* Δ*jmjc* double mutant strain was not restored for lesion formation on whole rice leaves (data not shown), thus constraining the role of MoJmjC, like MoSod1, to mediating the early events of epidermal rice cell infection. Taken together, these data suggest MoJmjC is a MoSir2-dependent negative regulator of *MoSOD1* gene expression.

How might MoJmjC regulate *MoSOD1* gene expression in a MoSir2-dependent manner? Informed by the proteomic, transcript and genetic data discussed above, we hypothesized that the acetylated MoJmjC protein found to accumulate in Δ*sir2* but not Guy11 samples [following growth in 1% GMM (Table S2) and 10% GMM (Tables 1 and 2 and Table S2)] might interact with the promoter of *MoSOD1* to repress transcription. To test this assumption, we generated Guy11 and Δ*sir2* strains expressing MoJmjC proteins fused at the C-terminal to the FLAG epitope (MoJmjC^{FLAG}), and performed chromatin immunoprecipitation (ChIP) studies on cross-linked DNA samples isolated from strains grown on 1% and 10% GMM using Anti-FLAG. This was followed by the quantification of *MoSOD1* DNA in MoJmjC^{FLAG} ChIP samples compared to negative controls using qRT-PCR. Growth on 10% GMM consistently failed to yield sufficient DNA for ChIP studies, but cross-linked DNA derived from MoJmjC^{FLAG} strains grown in 1% GMM was successfully immunoprecipitated by Anti-FLAG. Figure 8C shows how subsequent qRTPCR analysis detected an 18-fold enrichment of *MoSOD1* DNA above background levels in ChIP samples derived from Δ*sir2 MoJMJC^{FLAG}* strains. *MoSOD1* DNA enrichment was not detected above background levels in ChIP samples from Guy11 strains expressing MoJmjC^{FLAG} (Fig. 8C). This demonstrates that in Δ*sir2* strains, when MoJmjC is abundant and acetylated, MoJmjC is present at the *MoSOD1* promoter where it likely acts to repress gene expression.

When all the data are considered together, our results are consistent with the model of MoSir2 signaling shown in Fig. 8D whereby MoSir2, in a mechanism that might involve MoJmjC deacetylation, inactivates MoJmjC repression of the *MoSOD1* promoter in order to express *MoSOD1* and subsequently neutralize plant ROS to suppress rice defenses during infection (Fig. 8D).

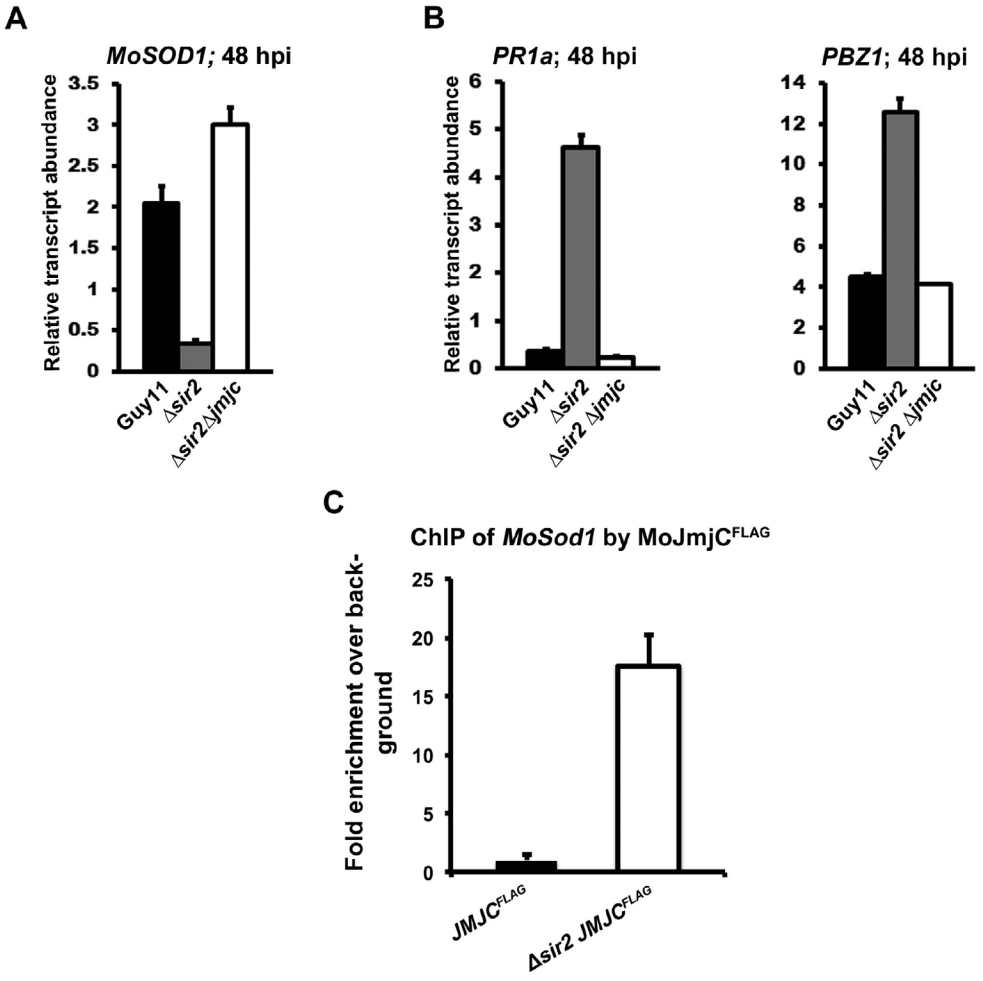

Fig. 8. Absence of MoJmjC is required for *MoSOD1* expression and the suppression of rice PR gene expression.

A. *MoSOD1* gene expression is elevated in Δ*sir2* Δ*jmjc* strains in rice cells compared to Δ*sir2* parental strains. Expression is given as the average of three independent measurements, normalized against *M. oryzae* actin gene expression. Error bars are SD.

B. The expression of *PR1a* and *PBZ1* genes were analyzed in rice cells infected with Δ*sir2* Δ*jmjc* strains compared to Guy11 and Δ*sir2* parental strains at 48 hpi. The values were normalized against *M. oryzae* actin expression. Error bars are SD.

C. MoJmjC associates with *MoSOD1* DNA in a MoSir2-dependent manner. Strains were grown for 16 h in 1% glucose media with 10 mM nitrate as the nitrogen source. Following ChIP, *MoSOD1* DNA was enriched 18-fold above background levels in samples derived from Δ*sir2* strains carrying MoJmjCFLAG (open bars). In contrast, samples from Guy11 strains carrying MoJmjCFLAG (closed bars) were not enriched for *MoSOD1* DNA compared to background following ChIP. Values are the mean of three independent replicates. Error bars are SD.

D. Proposed model for the regulation of plant defense suppression by MoSir2, via MoJmjC and MoSod1, during the early stages of infection.

Discussion

The blast fungus *M. oryzae* is a threat to rice and wheat harvests (Fernandez and Wilson, 2012), but its development as a model system (Dean *et al*., 2005; Fernandez and Wilson, 2014a) places it at the forefront of efforts to understand how plant infection is achieved at the molecular level. During rice infection, *M. oryzae* has an extended biotrophic growth phase that is facilitated by the correct physiological responses to available carbon sources (Fernandez *et al*., 2012), and by the secretion of effectors to re-program the host cell (Giraldo *et al*., 2013; Yi and Valent, 2013). In this study, we sought to uncover new information about how plant infection is regulated by targeting a *M. oryzae* sirtuin-encoding gene, *MoSIR2*, for gene deletion and analysis. Sirtuins are metabolic regulators controlling fundamental cell survival processes at the epigenetic level (Finkel *et al*., 2009; Houtkooper *et al*., 2012). Here, we have expanded the repertoire of this important class of enzymes to include mediation of the *M. oryzae*–rice interaction. Because MoSir2 is not involved in appressoria formation or function, the significance of this work lies in revealing MoSir2 as a hitherto unrecognized *in planta*-specific blast control point. MoSir2 is thus an attractive target for preventing rice disease, and future abrogation strategies might benefit from the wealth of knowledge generated in other systems where sirtuins are key players (Finkel *et al*., 2009; Houtkooper *et al*., 2012).

Loss of MoSir2 function resulted in strains attenuated for cell-to-cell growth due to impaired oxidative defenses and the concomitant elicitation of strong plant defense responses. The biotrophic growth of Δ*sir2* strains was restored by the addition of the NADPH oxidase inhibitor DPI. The concentration of DPI used did not affect appressorium formation (Fig. 5B) and was therefore not high enough to inhibit endogenous NADPH oxidase activity (Egan *et al*., 2007). These results thus confirm that, although MoSir2 might have additional unknown roles in the rice cell, the major function of MoSir2 is to regulate antioxidation in order to neutralize host-derived ROS and thereby facilitate the suppression of rice cell defenses during biotrophy. Interestingly, under optimal axenic growth conditions, *MoSIR2* expression was repressed by Tps1, suggesting a genetic link between these two regulators of antioxidation. Tps1 controls the production of NADPH by G6PDH in response to G6P binding (Wilson *et al*., 2007) in order, at least in part, to fuel the glutathione and thioredoxin antioxidation systems (Fernandez and Wilson, 2014b). Recently, deacetylation of G6PDH by SIRT2 in human cells has been shown to stimulate NADPH production in the pentose phosphate pathway (PPP) during oxidative stress (Wang *et al*., 2014). This raises the tantalizing possibility that in *M. oryzae*, Tps1 and MoSir2 regulation might converge on the PPP to modulate redox balance during oxidative stress. Testing this hypothesis and unpacking the *in planta* relationship(s) between Tps1 and MoSir2 will be a future goal of our work.

The restricted growth of Δ*sir2* strains in rice epidermal cells resulted at least in part from the loss of *MoSOD1* expression, and an Δ*sod1* deletion mutant mimicked Δ*sir2* strains for glucose intolerance (where it was the only SOD expressed under these conditions), sensitivity to oxidative stresses, and a reduced capacity to neutralize host ROS that was also accompanied by granular depositions and partial loss of plant defense gene suppression. How MoSod1 neutralizes host ROS is unknown. Although a *M. oryzae* catalase-peroxidase, CpxB, is secreted and required for neutralizing plant-derived ROS during early infection (but is not required for pathogenicity) (Tanabe *et al*., 2011), MoSod1 – like the host ROS-neutralizing enzymes glutathione reductase (Fernandez and Wilson, 2014b) and glutathione peroxidase (Huang *et al*., 2011) – is not predicted by SignalP to be secreted. Therefore, identifying the mechanisms by which these enzymes detoxify host ROS will likely be important areas of study with significance for understanding how plant-fungal interactions are mediated.

In addition to *MoSOD1*, MoSir2 was also shown to regulate the *in planta* expression of a likely Sod2- encoding gene, but its contribution to rice blast disease is currently on open question.

Oxidative defenses were restored in Δ*sir2* extragenic suppressor mutant strains that could grow on 10% GMM, suggesting loss of MoSir2 function in Δ*sir2* strains could be by-passed by second-site mutations. Subsequently, ATMT revealed *MoJMJC* to be one of at least two genes that might achieve this (Table 3). Indeed, *MoSOD1* expression was restored in Δ*sir2* strains that had lost MoJmjC function, and Δ*sir2* Δ*jmjc* double mutant strains could suppress plant defenses in epidermal cells. Thus, through the functional study of Δ*sir2*, Δ*sod1* and the Δ*sir2* Δ*jmjc* double mutant strains, and the demonstration by ChIP that MoJmjC binds the *MoSOD1* promoter in a MoSir2-dependent manner, we propose that *MoSOD1* expression requires MoJmjC inactivation – via MoSir2 in Guy11 or gene disruption in Δ*sir2* strains – in order for MoSod1 to neutralize host ROS and suppress plant defenses (Fig. 8D).

MoJmjC was acetylated in Δ*sir2* strains (Table 2) and carries a cupin-like domain with similarity to JmjC domains. JmjC-domain-containing proteins can function to modulate rRNA cap and/or ribonucleoprotein methylation (Klose *et al*., 2006) and can also catalyze lysine demethylation of histones via hydroxylation (Klose *et al*., 2006; Tsukada *et al*., 2006; Tsukada, 2012). MoJmjC was found by ChIP to physically associate with the *MoSOD1* promoter, although direct DNA binding is not predicted for this protein. Instead, MoJmjC might function as part of a co-repressing complex or by modulating the function of other DNA-binding proteins at the *MoSOD1* promoter. Indeed, two-step crosslinking (Nowak *et al*., 2005) was used when performing our ChIP experiments to take into account the likelihood that MoJmjC indirectly binds DNA. Taken together, we propose that MoSir2 does not regulate *MoSOD1* expression via histone modification but instead is required to deacetylate MoJmjC, thereby alleviating MoJmjC repression at the *MoSOD1*

promoter (Fig. 8D). The role of JmjC-domain proteins in catalyzing lysine demethylation of histones suggests the intriguing scenario that MoJmjC histone demethylase activity might be regulated by MoSir2-dependent deacetylation in order to influence gene expression at the *MoSOD1* promoter. Future studies will involve characterizing MoJmjC function and identifying MoJmjC-interacting proteins at the *MoSOD1* promoter in order to further articulate the mechanism of gene regulation by MoJmjC and MoSir2.

In conclusion, by coupling proteomic analyses with forward genetics and live-cell imaging, the work presented here has allowed us to dissect a genetic pathway regulating the suppression of host defense responses in rice epidermal cells. Consequently, this work might open up new lines of investigation into understanding plant infection by *M. oryzae* that could be extended to other important fungal pathosystems. This is timely considering fungal diseases of agronomically important crops are among some of the most recalcitrant problems we face as a species (Pennisi, 2010; Fisher *et al*., 2012).

Experimental procedures

Fungal strains and growth conditions

The mutant strains used throughout this study were generated from the wild-type *M. oryzae* strain Guy11 and stored at −20°C in the laboratory of R.A. Wilson at the University of Nebraska-Lincoln (Table S5). Standard growth conditions and storage procedures were performed as described previously (Fernandez *et al*., 2012; 2013). Wild type and all the mutants were propagated on complete media (CM) and growth tested on 1% glucose minimal media (1% GMM) with nitrate as sole nitrogen source, as previously described (Fernandez *et al*., 2012), unless otherwise stated. To generate oxidative, cell wall and osmotic stress conditions, we placed 5 mm diameter agar plugs of Guy11 and mutant strains into CM plates containing 5 mM and 10 mM hydrogen peroxide (H2O2, 30% in water; Fisher), 100 μg ml^{-1} Congo Red (Sigma), 0.5 M NaCl (Sigma) and 1 M sorbitol (Sigma) solutions. All plate images were taken with a Sony Cyber-shot digital camera, 14.1 mega pixels. Sporulation rates were measured from three independent CM plates as described previously (Wilson *et al*., 2012).

Pathogenicity and live-cell imaging assays

Three-week-old rice seedlings (*Oryza sativa* cultivar CO-39) were infected with conidia suspension of Guy11 or mutant strains (1×10^5 spores ml^{-1}) in a 0.20% gelatin (Difco) solution. Infected rice plants were incubated for 5 to 7 days at 24°C under 12 h dark/light cycles. Images of the infected leaves were taken using an Epson Workforce scanner at a resolution of 600 dpi.

Detached rice leaf sheath inoculations in the cultivar CO-39 were prepared as described previously (Wilson *et al*., 2012). Infected sheaths were analyzed using a Zeiss AxioSkop microscope. The average rate of appressorium formation on hydrophobic surface/leaf surface at 24 hpi, penetration at 30 hpi, and IH movement rate to adjacent cells at 48 hpi were performed as previously described (Fernandez *et al*., 2013). At 48 hpi, IH growth rate was measured using a four-point scale described previously (Wilson *et al*., 2012). Images were taken using a Nikon A1 laser scanning confocal mounted on a Nikon 90i compound microscope at the University of Nebraska-Lincoln Microscopy core facility.

The DAB staining assay were performed as previously described (Chi *et al*., 2009). For this assay we used rice sheaths from the susceptible cultivar CO-39. Briefly, rice sheath segments were inoculated with conidial suspensions of 5×10^4 spores ml^{-1} in a 0.20% gelatin solution. At 44 hpi, the infected sheaths were stained with 1 mg ml^{-1} 3,3′- diaminobenzidine solution (DAB, Sigma) in the dark for 8 h at room temperature. Then the samples were cleared with ethanol: acetic acid solution (94:4 v/v) for 2 h.

Targeted gene replacement

Targeted gene deletions were performed as previously described previously (Wilson *et al*., 2010). *MoSIR2* and *MoSOD1* were replaced in the Guy11 genome by the *ILV1* gene conferring resistance to sulphonyl urea. *MoJMJC* was replaced in the Δ*sir2* strain using the *Bar* gene conferring bialaphos resistance. Primers were designed as previously described (Wilson *et al*., 2010) (Table S6).

Complementation analysis

Complementation studies were performed using the yeast GAP-repair approach described in Zhou *et al*. (2011) and the primers in Table S6.

A. tumefaciens*-mediated transformation and TAIL-PCR*

Agrobacterium tumefaciens-mediated transformation (ATMT) was carried out according to Fernandez *et al*. (2012). To identify the T-DNA flanking sequences, TAIL-PCR was performed as previously described (Chen *et al*., 2011) using the primers in Table S6.

RNA extraction, qRT-PCR and fungal biomass quantification

Total RNA was isolated from infected plant tissues and frozen fungal mycelia using the RNeasy Plant Mini Kit (Qiagen) according to the manufacturer's instruction, following Fernandez *et al*. (2013). Fungal mycelia and leaf

samples were prepared and harvested as previously described (Fernandez *et al*., 2013). qRT-PCR reactions were performed as described previously (Fernandez *et al*., 2012) using the primers in Table S6. Ct (cycle threshold) values of each gene were normalized against *M. oryzae* actin (*MoACT1*), *O. sativa* actin (*OsACT*) or β-tubulin (*TUB2*) transcript levels. Fold changes were compared between treatments and strains. The analysis was conducted at least twice and from two independent biological replications. In order to quantify the relative abundance of fungal DNA in plant tissue, DNA was extracted from rice sheaths infected with Guy11 and Δ*sir2* strains at 48 hpi by using a HP fungal DNA mini Kit (Omega, BioTek). Specific primers for the *M. oryzae* and rice actin were used in this analysis.

Protein extraction

Strains were grown in CM for 48 h, then transferred to MM with nitrate for 16 h, following (Fernandez *et al*., 2012). Five hundred milligrams of fungal biomass (wet weight) was transferred in to a 1 ml lysis buffer comprising 8 M urea in 100 mM ammonium bicarbonate and containing 1.5 mM protease inhibitor (PMSF, Sigma). The biomass was then subjected to bead beating using a glass bead beater for 3 min at 4°C. The supernatant was collected after centrifugation at 10,000 *g* for 20 min. The proteins in the supernatant were precipitated by acetone and the resultant protein pellets were resuspended in 100 mM ammonium bicarbonate. The protein concentration was estimated using the BCA protein assay kit (Thermo Fisher Scientific). Extracted proteins were subjected to in-solution trypsin digestion. Briefly, the proteins were reduced with 10 mM dithiothreitol and alkylated with 40 mM iodoacetamide followed by trypsin (Roche) (1:50 trypsin : protein ratio) digestion overnight at 37°C. The tryptic peptides were desalted and concentrated using PepClean C-18 spin columns according to manufacturer's instructions (Thermo Scientific).

LC-MS/MS analysis

LC-MS/MS was performed with an ultimate 3000 Dionex MDLC system (Dionex Corporation, USA) integrated with a nanospray source and LCQ Fleet Ion Trap mass spectrometer (Thermofinnigan, USA). LC-MS/MS included an online sample pre-concentration and desalting using a monolithic C18 trap column (Pep Map, 300 µm I.D. × 5 mm, 100 Å, 5 µm, Dionex). The sample was loaded on to the monolithic trap column at a flow rate of 40 µl min^{-1}. The desalted peptides were then eluted and separated on a C18 Pep Map column (75 µm I.D. × 15 cm, 3 µm, 100 Å, New Objective, USA) by applying an acetonitrile (ACN) gradient (ACN plus 0.1% formic acid, 90 min gradient at a flow rate of 250 nl min^{-1}) and were introduced into the mass spectrometer

using the nano spray source. The LCQ Fleet mass spectrometer was operated with the following parameters: nano spray voltage, 2.0 kV; heated capillary temperature, 200°C; full scan m/z range, 400–2000). The mass spectrometer was operated in data-dependent mode with four MS/MS spectra for every full scan, five microscans averaged for full scans and MS/MS scans, a 3 m/z isolation width for MS/MS isolations, and 35% collision energy for collision-induced dissociation.

Database analysis

The acquired MS/MS spectra were searched against *M. oryzae* protein sequence databases using MASCOT (Version 2.2 Matrix Science, London, UK). Database search criteria were as follows: enzyme: trypsin, missed cleavages: 2; mass: monoisotropic; fixed modification: carbamidomethyl (C); peptide tolerance: 1.5 Da; MS/MS fragment ion tolerance: 1 Da. Acetylation of K, S and C (+42 Da) residues were set as variable modifications. Probability assessment of peptide assignments and protein identifications were accomplished by Scaffold (Scaffold 3.0 Proteome Software, Portland, OR). Criteria for protein identification included detection of at least 1 unique identified peptide and a peptide and protein probability score of ≥ 90. Relative quantification of the proteins was done based on the label-free method of spectral counting using the normalized spectral counts for each protein. Analysis of Gene ontology (GO) categories (biological process, cellular component and molecular function) of the identified proteins were done using Scaffold software.

Chromatin immunoprecipitation (ChIP)

JMJCFLAG was constructed following the protocol of Zhou *et al*. (2011) – using the vector pHZ126 and the primers in Table S6 – and integrated into the genome of Guy11 and Δ*sir2* strains. ChIP was performed as described by Kim and Mitchell (2011), with some modifications. Briefly, strains were grown in liquid CM for 48 h before switching to 1% and 10% GMM with 10 mM nitrate as the sole nitrogen source for 16 h. At least two biological replications were performed per strain. Strains used included Guy11 and Δ*sir2* with and without the *MoJMJCFLAG* allele. Guy11 and Δ*sir2* strains not carrying the *MoJMJCFLAG* allele were used to determine the background levels of *MoSOD1* DNA following ChIP. For each strain, mycelia was collected with Miracloth, washed thoroughly with distilled water, and incubated in the cross-linking buffer [comprising 20 mM HEPES, pH 7.4, 1 mM EDTA, 1 mM phenylmethylsulphonyl fluoride, and 2 mM disuccinimidyl glutarate (DSG, Thermo Scientific) (Nowak *et al*., 2005)] for 45 min at room temperature with gentle shaking. We performed twostep cross-linking, with formaldehyde

added to a final concentration of 1% for the last 20 min of cross-linking with DSG. Cross-linking was stopped by the addition of glycine to a final concentration of 0.125 M for 10 min incubation at room temperature. The mycelia were harvested with Miracloth, washed excessively with distilled water and flash frozen in liquid nitrogen. After grinding the cross-linked mycelia with pre-chilled mortar and pestle, the cross-linked DNA was isolated with the Plant Nuclear Isolation Kit (Sigma), resuspended in nuclear membrane lysis buffer [50 mM HEPES, pH 7.5, 150 mM NaCl, 1 mM EDTA, 1% Triton X-100, 0.1% deoxycholate, 0.1% SDS, 10 mM sodium butyrate, 1 mM PMSF, 1% (v/v) proteinase inhibitor cocktail (Sigma–Aldrich)] and subjected to sonication to obtain DNA fragments of 200–1000 bp. For ChIP, the nuclear lysates were first pre-cleared with Sepharose beads (4B200, Sigma) at 4°C for 4 h, and 25 µg chromatin was used to incubate with 20 µl of Anti-FLAG M2 Affinity Gel (A2220, Sigma) overnight at 4°C with gentle agitation. The normal Mouse IgG-Agarose (A0919, Sigma) was used as the negative control for non-specific binding and was processed in parallel. Thirty per cent of the DNA aliquot was saved and served as input chromatin for further analysis. After overnight incubation, the beads were washed four times in buffer (10 mM HEPES, pH 7.5, 150 mM NaCl, 0.1% Triton X-100), and the immune complexes were eluted with 100 µl of 3× FLAG peptide (F4799, Sigma) with a final concentration of 200 µg ml^{-1} in elution buffer (50 mM Tris-HCl, pH 7.5, 150 mM NaCl). For reverse cross-linking, the eluate was first digested with 0.2 mg ml^{-1} Proteinase K (Thermo) for 2 h at 45°C, then NaCl was added to a final concentration of 0.2 M and the mixture was incubated at 65°C overnight. After treatment with RNase A, DNAs were purified using Wizard PCR clean-up kit (Promega). The quantification of eluted *MoSOD1* DNA was performed at least in triplicate using qRT-PCR and the specific *MoSOD1* primer pairs listed in Table S6. Values obtained from Anti-FLAG immunoprecipitation were adjusted for non-specific DNA binding and precipitation using Anti-IgG and normalized against input DNA. Fold enrichment of *MoSOD1* DNA in MoJmjCFLAG ChIP samples is given relative to background levels of *MoSOD1*. Background *MoSOD1* levels were determined by processing, in parallel, samples from negative control strains lacking MoJmjCFLAG.

Acknowledgments — Funding for this work was provided by the National Science Foundation (IOS-1145347) and USDA-NIFA (2014-67013- 21559). Jessie Fernandez was supported by a Hardin Fellowship and a graduate student assistantship from the Department of Plant Pathology, University of Nebraska-Lincoln. We thank Christian Elowsky (of the Morrison Microscopy Core Research Facility, University of Nebraska-Lincoln) and Janet D. Wright for technical support.

Supporting information — Additional supporting information is attached to the repository cover page for this article.

References

Baidyaroy, D., Brosch, G., Ahn, J.H., Graessle, S., Wegener, S., Tonukari, N.J., *et al*. (2001) A gene related to yeast HOS2 histone deacetylase affects extracellular depolymerase expression and virulence in a plant pathogenic fungus. *Plant Cell* 13: 1609–1624.

Bause, A.S., and Haigis, M.C. (2013) SIRT3 regulation of mitochondrial oxidative stress. *Exp Gerontol* 48: 634– 639.

Blander, G., and Guarente, L. (2004) The Sir2 family of protein deacetylases. *Annu Rev Biochem* 73: 417–435.

Chen, X.L., Yang, J., and Peng, Y.L. (2011) Large scale insertional mutagenesis in *Magnaporthe oryzae* by *Agrobacterium tumefaciens*-mediated transformation. *Methods Mol Biol* 722: 213–224.

Chen, Y., Zhang, J., Lin, Y., Lei, Q., Guan, K.L., Zhao, S., *et al*. (2011) Tumour suppressor SIRT3 deacetylates and activates manganese superoxide dismutase to scavenge ROS. *EMBO Rep* 12: 534–541.

Chi, M.H., Park, S.Y., Kim, S., and Lee, Y.H. (2009) A novel pathogenicity gene is required in the rice blast fungus to suppress the basal defenses of the host. *PLoS Pathog* 5: e1000401.

Dagdas, Y.F., Yoshino, K., Dagdas, G., Ryder, L.S., Bielska, E., Steinberg, G., *et al*. (2012) Septin-mediated plant cell invasion by the rice blast fungus, *Magnaporthe oryzae*. *Science* 336: 1590–1595.

Dean, R.A., Talbot, N.J., Ebbole, D.J., Farman, M.L., Mitchell, T.K., Orbach, M.J., *et al*. (2005) The genome sequence of the rice blast fungus *Magnaporthe grisea*. *Nature* 434: 980–986.

Ding, S., Mehrabi, R., Koten, C., Kang, Z., Wei, Y., Seong, K., *et al*. (2009) Transducin beta-like gene FTL1 is essential for pathogenesis in *Fusarium graminearum*. *Eukaryot Cell* 8: 867–876.

Ding, S.L., Liu, W., Iliuk, A., Ribot, C., Vallet, J., Tao, A., *et al*. (2010) The Tig1 histone deacetylase complex regulates infectious growth in the rice blast fungus *Magnaporthe oryzae*. *Plant Cell* 22: 2495–2508.

Egan, M.J., Wang, Z.Y., Jones, M.A., Smirnoff, N., and Talbot, N.J. (2007) Generation of reactive oxygen species by fungal NADPH oxidases is required for rice blast disease. *Proc Natl Acad Sci USA* 104: 11772–11777.

Fernandez, J., and Wilson, R.A. (2012) Why no feeding frenzy? Mechanisms of nutrient acquisition and utilization during Infection by the rice blast fungus *Magnaporthe oryzae*. *Mol Plant Microbe Interact* 25: 1286–1293.

Fernandez, J., and Wilson, R.A. (2014a) Cells in cells: morphogenetic and metabolic strategies conditioning rice infection by the blast fungus *Magnaporthe oryzae*. *Protoplasma* 251: 37–47.

Fernandez, J., and Wilson, R.A. (2014b) Characterizing roles for the glutathione reductase, thioredoxin reductase and thioredoxin peroxidase-encoding genes of *Magnaporthe oryzae* during rice blast disease. *PLoS ONE* 9: e87300.

Fernandez, J., Wright, J.D., Hartline, D., Quispe, C.F., Madayiputhiya, N., and Wilson, R.A. (2012) Principles of carbon catabolite repression in the rice blast fungus: Tps1, Nmr1-3, and a MATE–Family Pump regulate glucose metabolism during Infection. *PLoS Genet* 8: e1002673.

Fernandez, J., Yang, K.T., Cornwell, K.M., Wright, J.D., and Wilson, R.A. (2013) Growth in rice cells requires de novo purine biosynthesis by the blast fungus *Magnaporthe oryzae*. *Sci Rep* 3: 2398.

Finkel, T., Deng, C.X., and Mostoslavsky, R. (2009) Recent progress in the biology and physiology of sirtuins. *Nature* 460: 587–591.

Fisher, M.C., Henk, D.A., Briggs, C.J., Brownstein, J.S., Madoff, L.C., McCraw, S.L., *et al*. (2012) Emerging fungal threats to animal, plant and ecosystem health. *Nature* 484: 186–194.

Frye, R.A. (2000) Phylogenetic classification of prokaryotic and eukaryotic Sir2-like proteins. *Biochem Biophys Res Commun* 273: 793–798.

Giraldo, M.C., Dagdas, Y.F., Gupta, Y.K., Mentlak, T.A., Yi, M., Martinez-Rocha, A.L., *et al*. (2013) Two distinct secretion systems facilitate tissue invasion by the rice blast fungus *Magnaporthe oryzae*. *Nat Commun* 4: 1996.

Gregoretti, I.V., Lee, Y.M., and Goodson, H.V. (2004) Molecular evolution of the histone deacetylase family: functional implications of phylogenetic analysis. *J Mol Biol* 338: 17–31.

Haigis, M.C., and Guarente, L.P. (2006) Mammalian sirtuins emerging roles in physiology, aging, and calorie restriction. *Genes Dev* 20: 2913–2921.

Haigis, M.C., and Sinclair, D.A. (2010) Mammalian sirtuins: biological insights and disease relevance. *Annu Rev Pathol* 5: 253–295.

Houtkooper, R.H., Pirinen, E., and Auwerx, J. (2012) Sirtuins as regulators of metabolism and healthspan. *Nat Rev Mol Cell Biol* 13: 225–238.

Huang, K., Czymmek, K.J., Caplan, J.L., Sweigard, J.A., and Donofrio, N.M. (2011) *HYR1*-mediated detoxification of reactive oxygen species is required for full virulence in the rice blast fungus. *PLoS Pathog* 7: e1001335.

Imai, S., Armstrong, C.M., Kaeberlein, M., and Guarente, L. (2000) Transcriptional silencing and longevity protein Sir2 is an NAD-dependent histone deacetylase. *Nature* 403: 795–800.

Kaeberlein, M., McVey, M., and Guarente, L. (1999) The SIR2/3/4 complex and SIR2 alone promote longevity in *Saccharomyces cerevisiae* by two different mechanisms. *Genes Dev* 13: 2570–2580.

Kankanala, P., Czymmek, K., and Valent, B. (2007) Roles for rice membrane dynamics and plasmodesmata during biotrophic invasion by the blast fungus. *Plant Cell* 19: 706– 724.

Khang, C.H., Berruyer, R., Giraldo, M.C., Kankanala, P., Park, S.-Y., Czymmek, K., *et al*. (2010) Translocation of *Magnaporthe oryzae* effectors into rice cells and their subsequent cell-to-cell movement. *Plant Cell* 22: 1388–1403.

Kim, S., and Mitchell, T.K. (2011) The application of ChIP-chip analysis in the rice blast pathogen. *Methods Mol Biol* 722: 121–131.

Kim, S.C., Sprung, R., Chen, Y., Xu, Y., Ball, H., Pei, J., *et al*. (2006) Substrate and functional diversity of lysine acetylation revealed by a proteomics survey. *Mol Cell* 23: 607–618.

Klose, R.J., Kallin, E.M., and Zhang, Y. (2006) JmjC-domain-containing proteins and histone demethylation. *Nat Rev Genet* 7: 715–727.

Koeck, M., Hardham, A.R., and Dodds, P.N. (2011) The role of effectors of biotrophic and hemibiotrophic fungi in infection. *Cell Microbiol* 13: 1849–1857.

Kops, G.J., Dansen, T.B., Polderman, P.E., Saarloos, I., Wirtz, K.W., Coffer, P.J., *et al*. (2002) Forkhead transcription factor FOXO3a protects quiescent cells from oxidative stress. *Nature* 419: 316–321.

Laluk, K., and Mengiste, T. (2010) Necrotroph attacks on plants: wanton destruction or covert extortion? *Arabidopsis Book* 8: e0136.

Li, Y., Wang, C., Liu, W., Wang, G., Kang, Z., Kistler, H.C., *et al*. (2011) The HDF1 histone deacetylase gene is important for conidiation, sexual reproduction, and pathogenesis in *Fusarium graminearum*. *Mol Plant Microbe Interact* 24: 487–496.

Lombard, D.B., Alt, F.W., Cheng, H.L., Bunkenborg, J., Streeper, R.S., Mostoslavsky, R., *et al*. (2007) Mammalian Sir2 homolog SIRT3 regulates global mitochondrial lysine acetylation. *Mol Cell Biol* 27: 8807–8814.

Miao, L., and St Clair, D.K. (2009) Regulation of superoxide dismutase genes: implications in disease. *Free Radic Biol Med* 47: 344–356.

Mosquera, G., Giraldo, M.C., Khang, C.H., Coughlan, S., and Valent, B. (2009) Interaction transcriptome analysis identifies *Magnaporthe oryzae* BAS1-4 as Biotrophy-associated secreted proteins in rice blast disease. *Plant Cell* 21: 1273–1290.

Nowak, D.E., Tian, B., and Brasier, A.R. (2005) Two-step cross-linking method for identification of NF-kappaB gene network by chromatin immunoprecipitation. *Biotechniques* 39: 715–725.

Outten, C.E., Falk, R.L., and Culotta, V.C. (2005) Cellular factors required for protection from hyperoxia toxicity in *Saccharomyces cerevisiae*. *Biochem J* 388: 93–101.

Pennisi, E. (2010) Armed and dangerous. *Science* 327: 804– 805.

Perfect, S.E., and Green, J.R. (2001) Infection structures of biotrophic and hemibiotrophic fungal plant pathogens. *Mol Plant Pathol* 2: 101–108.

Rine, J., Strathern, J.N., Hicks, J.B., and Herskowitz, I. (1979) A suppressor of mating-type locus mutations in *Saccharomyces cerevisiae*: evidence for and identification of cryptic mating-type loci. *Genetics* 93: 877–901.

Schwer, B., and Verdin, E. (2008) Conserved metabolic regulatory functions of sirtuins. *Cell Metab* 7: 104–112.

Spanu, P.D. (2012) The genomics of obligate (and nonobligate) biotrophs. *Annu Rev Phytopathol* 50: 91–109.

Tanabe, S., Ishii-Minami, N., Saitoh, K., Otake, Y., Kaku, H., Shibuya, N., *et al*. (2011) The role of catalase-peroxidase secreted by *Magnaporthe oryzae* during early infection of rice cells. *Mol Plant Microbe Interact* 24: 163–171.

Tanner, K.G., Landry, J., Sternglanz, R., and Denu, J.M. (2000) Silent information regulator 2 family of NAD-dependent histone/protein deacetylases generates a unique product, 1-O-acetyl-ADP-ribose. *Proc Natl Acad Sci USA* 97: 14178–14182.

Tsukada, Y. (2012) Hydroxylation mediates chromatin demethylation. *J Biochem (Tokyo)* 151: 229–246.

Tsukada, Y., Fang, J., Erdjument-Bromage, H., Warren, M.E., Borchers, C.H., Tempst, P., *et al*. (2006) Histone demethylation by a family of JmjC domain-containing proteins. *Nature* 439: 811–816.

Tucker, S.L., Besi, M.I., Galhano, R., Franceschetti, M., Goetz, S., Lenhert, S., *et al*. (2010) Common genetic pathways regulate organ-specific infection-related development in the rice blast fungus. *Plant Cell* 22: 953–972.

Wang, Y., and Tissenbaum, H.A. (2006) Overlapping and distinct functions for a *Caenorhabditis elegans* SIR2 and DAF-16/FOXO. *Mech Ageing Dev* 127: 48–56.

Wang, Y.P., Zhou, L.S., Zhao, Y.Z., Wang, S.W., Chen, L.L., Liu, L.X., *et al*. (2014) Regulation of G6PD acetylation by SIRT2 and KAT9 modulates NADPH homeostasis and cell survival during oxidative stress. *EMBO J* 33: 1304–1320.

Webster, B.R., Lu, Z., Sack, M.N., and Scott, I. (2012) The role of sirtuins in modulating redox stressors. *Free Radic Biol Med* 52: 281–290.

Wilson, R.A., and Talbot, N.J. (2009) Under pressure: investigating the biology of plant infection by *Magnaporthe oryzae*. *Nat Rev Microbiol* 7: 185–195.

Wilson, R.A., Jenkinson, J.M., Gibson, R.P., Littlechild, J.A., Wang, Z.-Y., and Talbot, N.J. (2007) Tps1 regulates the pentose phosphate pathway, nitrogen metabolism and fungal virulence. *EMBO J* 26: 3673–3685.

Wilson, R.A., Gibson, R.P., Quispe, C.F., Littlechild, J.A., and Talbot, N.J. (2010) An NADPH-dependent genetic switch regulates plant infection by the rice blast fungus. *Proc Natl Acad Sci USA* 107: 21902–21907.

Wilson, R.A., Fernandez, J., Quispe, C.F., Gradnigo, J., Seng, A., Moriyama, E., *et al*. (2012) Towards defining nutrient conditions encountered by the rice blast fungus during host infection. *PLoS ONE* 7: e47392.

Yang, X.J., and Grégoire, S. (2007) Metabolism, cytoskeleton and cellular signalling in the grip of protein Nε- and O-acetylation. *EMBO Rep* 8: 556–562.

Yang, X.J., and Seto, E. (2007) HATs and HDACs: from structure, function and regulation to novel strategies for therapy and prevention. *Oncogene* 26: 5310–5318.

Yi, M., and Valent, B. (2013) Communication between filamentous pathogens and plants at the biotrophic Interface. *Annu Rev Phytopathol* 51: 27.1–27.25.

Zhang, Z., Yang, Z., Zhu, B., Hu, J., Liew, C.W., Zhang, Y., *et al*. (2012) Increasing glucose 6-phosphate dehydrogenase activity restores redox balance in vascular endothelial cells exposed to high glucose. *PLoS ONE* 7: e49128.

Zhou, X., Li, G., and Xu, J.R. (2011) Efficient approaches for generating GFP fusion and epitope-tagging constructs in filamentous fungi. *Methods Mol Biol* 722: 199–212.